

1      Bayesian inference of relative fitness on high-throughput  
2                        pooled competition assays

3      Manuel Razo-Mejia<sup>1,\*</sup>, Madhav Mani<sup>3,4</sup>, and Dmitri Petrov<sup>1,2,5</sup>

4                       <sup>1</sup>*Department of Biology, Stanford University*

5                       <sup>2</sup>*Stanford Cancer Institute, Stanford University School of Medicine*

6                       <sup>3</sup>*NSF-Simons Center for Quantitative Biology, Northwestern University*

7                       <sup>4</sup>*Department of Molecular Biosciences, Northwestern University*

8                       <sup>5</sup>*Chan Zuckerberg Biohub*

9

10     The tracking of lineage frequencies via DNA barcode sequencing enables the  
11       quantification of microbial fitness. However, experimental noise coming from  
12       biotic and abiotic sources complicates the computation of a reliable inference.  
13       We present a Bayesian pipeline to infer relative microbial fitness from high-  
14       throughput lineage tracking assays. Our model accounts for multiple sources of  
15       noise and propagates uncertainties throughout all parameters in a systematic way.  
16       Furthermore, using modern variational inference methods based on automatic  
17       differentiation, we are able to scale the inference to a large number of unique  
18       barcodes. We extend this core model to analyze multi-environment assays,  
19       replicate experiments, and barcodes linked to genotypes. On simulations, our  
20       method recovers known parameters within posterior credible intervals. This  
21       work provides a generalizable Bayesian framework to analyze lineage tracking  
22       experiments. The accompanying open-source software library enables the adoption  
23       of principled statistical methods in experimental evolution.

24      **Introduction**

25     The advent of DNA barcoding—the ability to uniquely identify cell lineages with DNA  
26       sequences integrated at a specific locus—and high-throughput sequencing has opened new  
27       venues for understanding microbial evolutionary dynamics with an unprecedented level of  
28       temporal resolution<sup>1–3</sup>. These experimental efforts rely on our ability to reliably infer the  
29       relative fitness of an ensemble of diverse genotypes. Moreover, inferring these fitness values

30 over an ensemble of environmental conditions can help us determine the phenotypic diversity  
31 of a rapid adaptation process<sup>4</sup>.

32 As with any other sequencing-based quantification, tracking lineages via DNA barcode  
33 sequencing is inexorably accompanied by noise sources coming from experimental manipulation  
34 of the microbial cultures, DNA extraction, and sequencing library preparation that involves  
35 multiple rounds of PCR amplification, and the sequencing process itself. Thus, accounting for  
36 the uncertainty when inferring the relevant parameters from the data is a crucial step to draw  
37 reliable conclusions. Bayesian statistics presents a paradigm by which one can account for all  
38 known sources of uncertainty in a principled way<sup>5</sup>. This, combined with the development  
39 of modern Markov Chain Monte Carlo sampling algorithms<sup>6</sup> and approximate variational  
40 approaches<sup>7</sup> have boosted a resurgence of Bayesian methods in different fields<sup>8</sup>.

41 We present a Bayesian inference pipeline to quantify the uncertainty about the parametric  
42 information we can extract from high-throughput competitive fitness assays given a model  
43 of the data generation process and experimental data. In these assays, the fitness of an  
44 ensemble of genotypes is determined relative to a reference genotype<sup>3,4</sup>. Figure 1(A) shows a  
45 schematic of the experimental procedure in which an initial pool of barcoded strains are mixed  
46 with a reference strain and inoculated into fresh media. After some time—usually, enough  
47 time for the culture to saturate—an aliquot is transferred to fresh media, while the remaining  
48 culture is used for DNA sequencing of the lineage barcodes. The time-series information of  
49 the relative abundance of each lineage, i.e., the barcode frequency depicted in Figure 1(B), is  
50 used to infer the relative fitness—the growth advantage on a per-cycle basis—for each lineage  
51 with respect to the reference strain. The proposed statistical model accounts for multiple  
52 sources of uncertainty when inferring the lineages' relative fitness values (see Section for  
53 details on sources of uncertainty accounted for by the model). Furthermore, minor changes  
54 to the core statistical model allow us to account for relevant experimental variations of these  
55 competition assays. More specifically, in Section , we present a variation of the statistical  
56 model to infer fitness on growth dilution cycles in multiple environments with proper error  
57 propagation. Furthermore, as described in Section , our statistical model can account for  
58 batch-to-batch differences when jointly analyzing multiple experimental replicates using a  
59 Bayesian hierarchical model. Finally, a variant of these hierarchical models, presented in  
60 Section , can account for variability within multiple barcodes mapping to equivalent genotypes  
61 within the same experiment.

62 For all the model variations presented in this paper, we benchmark the ability of our pipeline  
63 to infer relative fitness parameters against synthetic data generated from logistic growth  
64 simulations with added random noise. A Julia package accompanies the present method to  
65 readily implement the inference pipeline with state-of-the-art scientific computing software.

66 **Results**

67 **Experimental setup**

68 The present work is designed to analyze time-series data of relative abundance of multiple  
69 microbial lineages uniquely identified by a DNA barcode<sup>3,4</sup>. In these competition assays, an  
70 ensemble of genotypes is pooled together with an unlabeled reference strain that, initially,  
71 represents the vast majority ( $\geq 90\%$ ) of the cells in the culture (see schematic in Figure 1(A)).  
72 Furthermore, a fraction of labeled genotypes equivalent to the unlabeled reference strain—  
73 hereafter defined as *neutral* lineages—are spiked in at a relatively high abundance ( $\approx 3 - 5\%$ ).  
74 The rest of the culture is left for the ensemble of genotypes of interest.

75 To determine the relative fitness of the ensemble of genotypes, a series of growth-dilution  
76 cycles are performed on either a single or multiple environments. In other words, the cultures  
77 are grown for some time; then, an aliquot is inoculated into fresh media for the next growth  
78 cycle. This process is repeated for roughly 4-7 cycles, depending on the initial abundances of  
79 the mutants and their relative growth rates. The DNA barcodes are sequenced at the end of  
80 each growth cycle to quantify the relative abundance of each of the barcodes. We point the  
81 reader to Kinsler et al. [4] for specific details on these assays for *S. cerevisiae* and to Ascensao  
82 et al. [3] for equivalent assays for *E. coli*. Figure 1(B) presents a typical barcode trajectory  
83 where the black trajectories represent the so-called *neutral* lineages, genetically equivalent  
84 to the untagged ancestor strain that initially dominates the culture. These spiked-in neutral  
85 lineages simplify the inference problem since the fitness metric of all relevant barcodes is  
86 quantified with respect to these barcodes—thus referred to as *relative fitness*.

87 **Preliminaries on mathematical notation**

88 Before jumping directly into the Bayesian inference pipeline, let us establish the mathematical  
89 notation used throughout this paper. We define (column) vectors as underlined lowercase  
90 symbols such as

$$\underline{x} = \begin{bmatrix} x_1 \\ x_2 \\ \vdots \\ x_N \end{bmatrix}. \quad (1)$$

91 In the same way, we define matrices as double-underline uppercase symbols such as

$$\underline{\underline{A}} = \begin{bmatrix} A_{11} & A_{12} & \cdots & A_{1N} \\ A_{21} & A_{22} & \cdots & A_{2N} \\ \vdots & \vdots & \ddots & \vdots \\ A_{M1} & A_{M2} & \cdots & A_{MN} \end{bmatrix}. \quad (2)$$

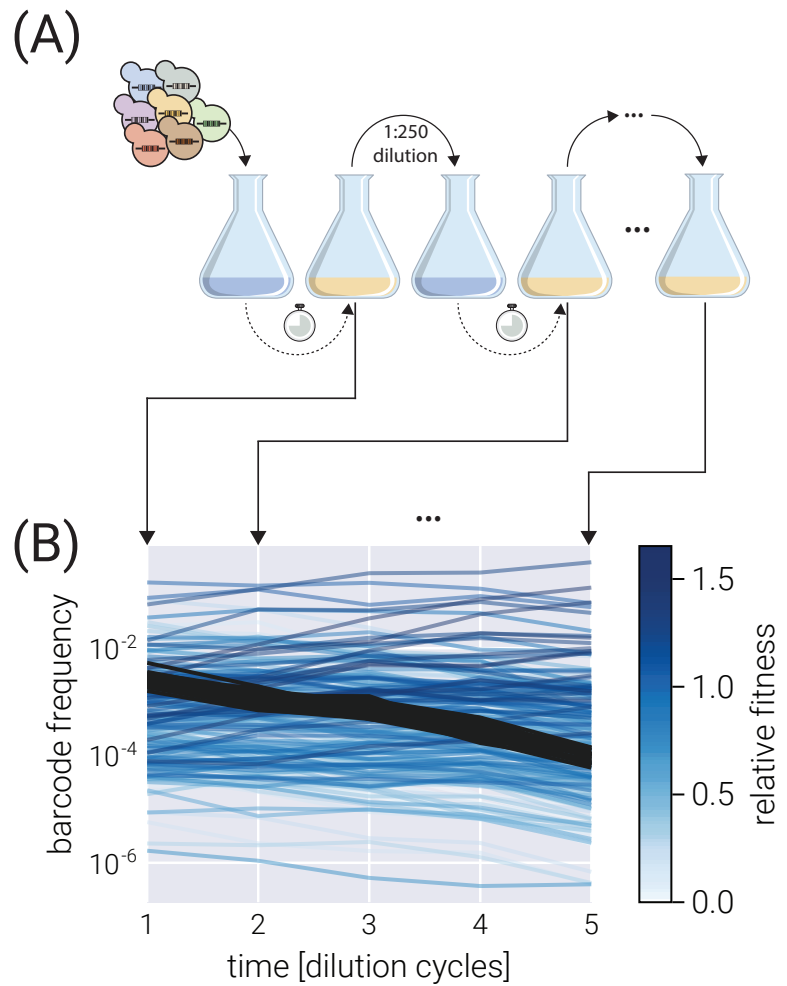


**Figure 1. Typical competitive fitness experiment.** (A) Schematic of the typical experimental design to determine the competitive fitness of an ensemble of barcoded genotypes. Genotypes are pooled together and grown over multiple growth-dilution cycles. At the end of each cycle, a sample is processed to generate a library for amplicon sequencing. (B) Typical barcode trajectory dataset. From each time point, the relative frequency of each barcode is determined from the total number of reads. Shades of blue represent different relative fitness. Darker gray lines define the typical trajectory of neutral lineages.

92 **Fitness model**

93 Empirically, each barcode frequency trajectory follows an exponential function of the  
 94 form<sup>1,3,4</sup>

$$f_{t+1}^{(b)} = f_t^{(b)} e^{(s^{(b)} - \bar{s}_t)\tau}, \quad (3)$$

95 where  $f_t^{(b)}$  is the frequency of barcode  $b$  at the end of cycle number  $t$ ,  $s^{(b)}$  is the relative  
 96 fitness with respect to the reference strain—the quantity we want to infer from the data— $\bar{s}_t$   
 97 is the mean fitness of the culture at the end of cycle number  $t$ , and  $\tau$  is the time pass between  
 98 cycle  $t$  and  $t + 1$ . We can rewrite Equation 3 as

$$\frac{1}{\tau} \ln \frac{f_{t+1}^{(b)}}{f_t^{(b)}} = (s^{(b)} - \bar{s}_t). \quad (4)$$

99 Equation 4 separates the measurements—the barcode frequencies—from the unobserved  
 100 (sometimes referred to as latent) parameters we want to infer from the data—the population  
 101 mean fitness and the barcode relative fitness. This is ultimately the functional form used  
 102 in our inference pipeline. Therefore, the relative fitness is computed by knowing the log  
 103 frequency ratio of each barcode throughout the growth-dilution cycles.

104 The presence of the neutral lineages facilitates the determination of the population mean  
 105 fitness value  $\bar{s}_t$ . Since every relative fitness is determined relative to the neutral lineage  
 106 that dominates the culture, we define their fitness to be  $s^{(n)} = 0$ , where the superscript  $(n)$   
 107 specifies their neutrality. This means that Equation 4 for a neutral lineage takes the simpler  
 108 form

$$\frac{1}{\tau} \ln \frac{f_{t+1}^{(n)}}{f_t^{(n)}} = -\bar{s}_t. \quad (5)$$

109 Therefore, we can use the data from these reference barcodes to directly infer the value of  
 110 the population mean fitness.

111 It is important to notice that the frequencies  $f_t^{(b)}$  are not the allele frequencies in the population  
 112 (most of the culture is not sequenced since the reference strain is not barcoded), but rather  
 113 the relative frequencies in the total number of sequencing reads. A way to conceptualize this  
 114 subtle but important point is to assume exponential growth in the *number of cells*  $N_t^{(b)}$  of  
 115 the form

$$N_{t+1}^{(b)} = N_t^{(b)} e^{\lambda^{(b)}\tau}, \quad (6)$$

116 for every barcode  $b$  with growth rate  $\lambda^{(b)}$ . However, when we sequence barcodes, we do not  
 117 directly measure the number of cells, but some number of reads  $r_t^{(b)}$  that map to barcode  $b$ .  
 118 In the simplest possible scenario, we assume

$$r_t^{(b)} \propto N_t^{(b)}, \quad (7)$$

119 where, importantly, the proportionality constant depends on the total number of reads for  
 120 the library for cycle  $t$ , which might vary from library to library. Therefore, to compare the

121 number of reads between libraries at different time points, we must normalize the number of  
 122 reads to the same scale. The simplest form is to define a relative abundance, i.e., a frequency  
 123 with respect to the total number of reads,

$$f_t^{(b)} \equiv \frac{r_t^{(b)}}{\sum_{b'} r_t^{(b')}}. \quad (8)$$

124 This is the frequency Equation 3 describes.

125 Our ultimate objective is to infer the relative fitness  $s^{(b)}$  for each of the  $M$  relevant barcodes  
 126 in the experiment—hereafter referred to as  $s^{(m)}$  to distinguish from the general  $s^{(b)}$  and the  
 127 neutral lineages  $s^{(n)}$  relative fitness. To do so, we account for the three primary sources of  
 128 uncertainty in our model:

- 129 1. Uncertainty in the determination of frequencies. Our model relates frequencies between  
 130 adjacent growth-dilution cycles to the fitness of the corresponding strain. However, we  
 131 do not directly measure frequencies. Instead, our data for each barcode consists of a  
 132 length  $T$  vector of counts  $\underline{r}^{(b)}$  for each of the  $T$  cycles in which the measurements were  
 133 taken.
- 134 2. Uncertainty in the value of the population mean fitness. We define neutral lineages  
 135 to have fitness  $s^{(n)} = 0$ , helping us anchor the value of the population mean fitness  
 136  $\bar{s}_t$  for each pair of adjacent growth cycles. Moreover, we take this parameter as an  
 137 empirical parameter to be obtained from the data, meaning that we do not impose a  
 138 functional form that relates  $\bar{s}_t$  to  $\bar{s}_{t+1}$ . Thus, we must infer the  $T - 1$  values of this  
 139 population mean fitness with their uncertainty that must be propagated to the value of  
 140 the mutants' relative fitness.
- 141 3. Uncertainty in each of the mutants' fitness values.

142 To account for all these sources of uncertainty in a principled way, in the next section, we  
 143 develop a Bayesian inference pipeline.

## 144 Bayesian inference

145 As defined in Section , our ultimate objective is to infer the vector of relative fitness values

$$\underline{s}^M = (s^{(1)}, s^{(2)}, \dots, s^{(M)})^\dagger, \quad (9)$$

146 where  $\dagger$  indicates the transpose. Our data consists of an  $T \times B$  matrix  $\underline{\underline{R}}$ , where  $B = M + N$   
 147 is the number of unique barcodes given by the sum of the number of unique, relevant barcodes  
 148 we care about,  $M$ , and the number of unique neutral barcodes,  $N$ , and  $T$  is the number of  
 149 growth cycles where measurements were taken. The data matrix is then of the form

$$\underline{\underline{R}} = \begin{bmatrix} - & r_1 & - \\ - & r_2 & - \\ \vdots & & \\ - & r_T & - \end{bmatrix}, \quad (10)$$

150 where each row  $\underline{r}_t$  is a  $B$ -dimensional array containing the raw barcode counts at cycle  $t$ . We  
 151 can further split each vector  $\underline{r}_t$  into two vectors of the form

$$\underline{r}_t = \begin{bmatrix} \underline{r}_t^N \\ \underline{r}_t^M \end{bmatrix}, \quad (11)$$

152 i.e., the vector containing the neutral lineage barcode counts  $\underline{r}_t^N$  and the corresponding vector  
 153 containing the mutant barcode counts  $\underline{r}_t^M$ . Following the same logic, matrix  $\underline{\underline{R}}$  can be split  
 154 into two matrices as

$$\underline{\underline{R}} = \begin{bmatrix} \underline{\underline{R}}^N & \underline{\underline{R}}^M \end{bmatrix}, \quad (12)$$

155 where  $\underline{\underline{R}}^N$  is a  $T \times N$  matrix with the barcode reads time series for each neutral lineage and  
 156  $\underline{\underline{R}}^M$  is the equivalent  $T \times M$  matrix for the non-neutral lineages.

157 Our objective is to compute the joint probability distribution for all relative fitness values  
 158 given our data. We can express this joint posterior distribution using Bayes theorem as

$$\pi(\underline{s}^M | \underline{\underline{R}}) = \frac{\pi(\underline{\underline{R}} | \underline{s}^M)\pi(\underline{s}^M)}{\pi(\underline{\underline{R}})}, \quad (13)$$

159 where hereafter  $\pi(\cdot)$  defines a probability density function. When defining our statistical  
 160 model, we need not to focus on the denominator on the right-hand side of Equation 13. Thus,  
 161 we can write

$$\pi(\underline{s}^M | \underline{\underline{R}}) \propto \pi(\underline{\underline{R}} | \underline{s}^M)\pi(\underline{s}^M). \quad (14)$$

162 However, when implementing the model computationally, the normalization constant on the  
 163 right-hand side of Equation 13 must be computed. This can be done from the definition of  
 164 the model via an integral of the form

$$\pi(\underline{\underline{R}}) = \int d^M \underline{s}^M \pi(\underline{\underline{R}} | \underline{s}^M)\pi(\underline{s}^M), \quad (15)$$

165 also known as a marginalization integral. Hereafter, differentials of the form  $d^n$  imply a  
 166  $n$ -dimensional integral.

167 Although Equation 13 and Equation 14 seem simple enough, recall that Equation 3 relates  
 168 barcode frequency values and the population mean fitness to the mutant relative fitness.  
 169 Therefore, we must include these nuisance parameters as part of our inference problem. We  
 170 direct the reader to the supplementary materials for the exact definitions of these parameters.  
 171 Here, it suffices to say that the inference problem must include the vector  $\bar{s}_T$  of all population  
 172 mean fitness values and the matrix  $\underline{\underline{F}}$  of all barcode frequencies within the sequencing data.  
 173 With these nuisance variables in hand, the full inference problem we must solve takes the  
 174 form

$$\pi(\underline{s}^M, \bar{s}_T, \underline{\underline{F}} | \underline{\underline{R}}) \propto \pi(\underline{\underline{R}} | \underline{s}^M, \bar{s}_T, \underline{\underline{F}})\pi(\underline{s}^M, \bar{s}_T, \underline{\underline{F}}). \quad (16)$$

175 To recover the marginal distribution over the non-neutral barcodes relative fitness values, we  
 176 can numerically integrate out all nuisance parameters, i.e.,

$$\pi(\underline{s}^M | \underline{\underline{R}}) = \int d^{T-1} \bar{s}_T \int d^B f_1 \cdots \int d^B f_T \pi(\underline{s}^M, \bar{s}_T, \underline{\underline{F}} | \underline{\underline{R}}). \quad (17)$$

177 **Factorizing the posterior distribution**

178 The left-hand side of Equation 16 is extremely difficult to work with. However, we can take  
179 advantage of the structure of our inference problem to rewrite it in a more manageable form.  
180 Specifically, the statistical dependencies of our observations and latent variables allow us  
181 to factorize the joint distribution into the product of multiple conditional distributions. To  
182 gain some intuition about this factorization, let us focus on the inference of the population  
183 mean fitness values  $\bar{s}_T$ . Equation 5 relates the value of the population mean fitness to the  
184 neutral lineage frequencies and nothing else. This suggests that when writing the posterior  
185 for these population mean fitness parameters, we should be able to condition it only on the  
186 neutral lineage frequency values, i.e.,  $\pi(\bar{s}_T | \underline{F}^N)$ . We point the reader to Section for the  
187 full mathematical details on this factorization. For our purpose here, it suffices to say we  
188 can rewrite the joint probability distribution as a product of conditional distributions of the  
189 form

$$\pi(\underline{s}^M, \bar{s}_T, \underline{F} | \underline{R}) = \pi(\underline{s}^M | \bar{s}_T, \underline{F}^M) \pi(\bar{s}_T | \underline{F}^N) \pi(\underline{F} | \underline{R}). \quad (18)$$

190 Written in this form, Equation 18 captures the three sources of uncertainty listed in Section in  
191 each term. Starting from right to left, the first term on the right-hand side of Equation 18  
192 accounts for the uncertainty when inferring the frequency values given the barcode reads.  
193 The second term accounts for the uncertainty in the values of the mean population fitness  
194 at different time points. The last term accounts for the uncertainty in the parameter we  
195 care about—the mutants' relative fitnesses. We refer the reader to Section for an extended  
196 description of the model with specific functional forms for each term on the left-hand side  
197 of Equation 18 as well as the extension of the model to account for multiple experimental  
198 replicates or hierarchical genotypes.

199 **Variational Inference**

200 One of the technical challenges to the adoption of Bayesian methods is the analytical in-  
201 tractability of integrals such as that of Equation 17. Furthermore, even though efficient  
202 Markov Chain Monte Carlo (MCMC) algorithms such as Hamiltonian Montecarlo can numeri-  
203 cally perform this integration<sup>6</sup>, the dimensionality of the problem in Equation 18 makes an  
204 MCMC-based approach prohibitively slow.

205 To overcome this computational limitation, we rely on the recent development of the automatic  
206 differentiation variational inference algorithm (ADVI)<sup>7</sup>. Briefly, when performing ADVI, our  
207 target posterior distribution  $\pi(\theta | \underline{R})$ , where  $\theta = (\underline{s}^M, \bar{s}_T, \underline{F})$ , is replaced by an approximate  
208 posterior distribution  $q_\phi(\theta)$ , where  $\phi$  fully parametrizes the approximate distribution. As  
209 further explained in Section , the numerical integration problem is replaced by an optimization  
210 problem of the form

$$q_\phi^*(\theta) = \min_{\phi} D_{KL}(q_\phi(\theta) || \pi(\theta | \underline{R})), \quad (19)$$

211 where  $D_{KL}$  is the Kulback-Leibler divergence. In other words, the complicated high-  
212 dimensional numerical integration problem is transformed into a much simpler problem

213 of finding the value of the parameters  $\phi$  such that Equation S4 is satisfied as best as possible  
214 within some finite computation time. Although to compute Equation S4, we require the  
215 posterior distribution we are trying to approximate  $\pi(\theta | \underline{R})$ , it can be shown that maximiz-  
216 ing the so-called evidence lower bound (ELBO)<sup>9</sup>—equivalent to minimizing the variational  
217 free energy<sup>10</sup>—is mathematically equivalent to performing the optimization prescribed by  
218 Equation S4. We direct the reader to Section for a short primer on variational inference.

219 This work is accompanied by the Julia library BarBay.jl that makes use of the implementation  
220 of both MCMC-based integration as well as ADVI optimization to numerically approximate  
221 the solution of Equation 17 within the Julia ecosystem<sup>11</sup>.

## 222 Inference on a single dataset

223 To assess the inference pipeline performance, we applied it to a simulated dataset with known  
224 ground truth relative fitness values (See Section for details on simulation). Figure 2(A)  
225 shows the structure of the synthetic dataset. The majority of barcodes of interest (faint  
226 color lines) are adaptive compared to the neutral barcodes ( $s^{(m)} > 0$ ). Although the barcode  
227 frequency trajectories look relatively smooth, our fitness model requires the computation of  
228 the log frequency ratio between adjacent time points as derived in Equation 4. Figure 2(B)  
229 shows such data transformation where we can better appreciate the observational noise input  
230 into our statistical model. This noise is evident for the darker lines representing the neutral  
231 barcodes since all of these lineages are assumed to be identically distributed.

232 To visualize the performance of our inference pipeline in fitting our fitness model to the  
233 observed data, we compute the so-called posterior predictive checks (PPC). In short, the  
234 PPC consists of repeatedly generating synthetic datasets in agreement with the results from  
235 the inference results. In other words, we use the resulting parameter values from the ADVI  
236 inference to generate possible datasets in agreement with the inferred values (See Section for  
237 further details on these computations). Figure 2(C) shows these results for all neutral lineages  
238 (upper left corner plot) and a few representative non-neutral barcodes. The different color  
239 shades represent the 95%, 68%, and 5% credible regions, i.e., the regions where we expect  
240 to find the data with the corresponding probability—or in terms of our parameter, the  $X\%$   
241 credible region is the interval where we expect the true parameter value to lie with  $X\%$   
242 probability.

243 The main advantage of our method is this natural interpretability of these credible regions  
244 where an  $X\%$  credible region indeed captures the region of parameter space where we expect  
245 with  $X\%$  probability the actual value of the parameter lies given our statistical model, our  
246 prior information, and the observed experimental data. A common mistake in the literature  
247 is interpreting frequentist confidence intervals as Bayesian credible regions when they are  
248 not equivalent<sup>12</sup>. Frequentist confidence intervals and Bayesian credible regions are based  
249 on fundamentally different philosophical approaches to statistics. Frequentist confidence  
250 intervals represent the range of values that would contain the true population parameter with  
251 a certain probability if the experiment was repeated many times. The confidence interval

252 does not represent the probability that the interval contains the true value. According to  
 253 a specific model and prior information, Bayesian credible regions represent the range of  
 254 values that contain the parameter with a certain posterior probability. The credible region  
 255 directly represents the probability that the region contains the true value. So, frequentist  
 256 confidence intervals cannot be interpreted as Bayesian credible regions because they have  
 257 fundamentally different meanings. Treating an  $X\%$  confidence interval like an  $X\%$  credible  
 258 region is fallacious since confidence intervals do not represent probabilistic coverage of the true  
 259 value like credible regions. The intervals are generated through entirely different procedures.

260 To capture the global performance of the model, Figure 2(D) compares the known ground  
 261 truth with the inferred relative fitness value for all barcodes of interest. There is an excellent  
 262 degree of correspondence between these values, with the error bars representing the 68%  
 263 credible region for the parameter value crossing the identity line for most barcodes. This  
 264 latter point is made clear with Figure 2(E) where  $\approx 90\%$  of ground truth fitness values fall  
 265 within one standard deviation of the mean in the inferred posterior distributions.

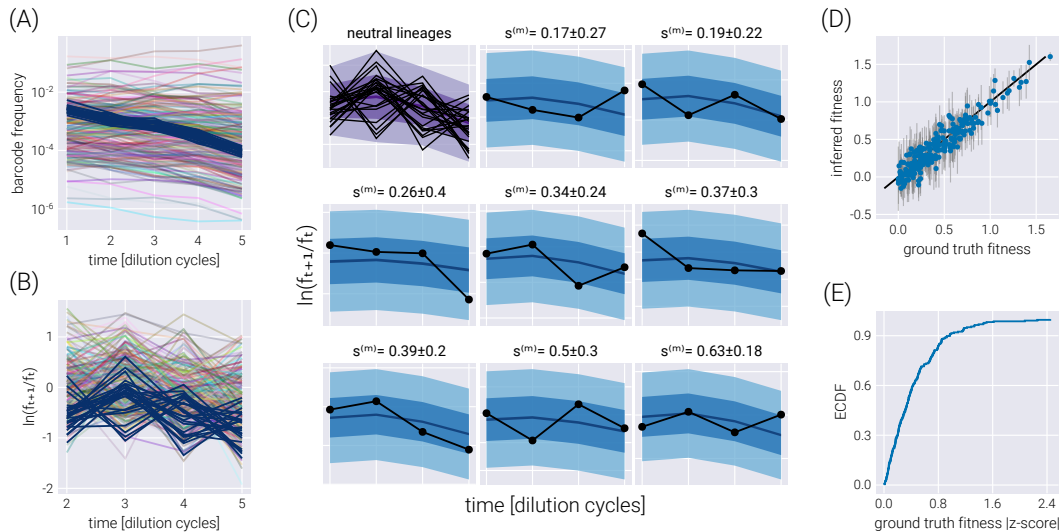


**Figure 2. Single dataset inference.** (A) Frequency trajectories that represent the raw data going into the inference. (B) Log frequency ratio between two adjacent time points used by the inference pipeline. Darker lines represent the neutral barcodes. These transformed data are much more noisy than the seemingly smooth frequency trajectories. (C) Examples of the posterior predictive checks for all neutral lineages (upper left panel) and a subset of representative mutant lineages. Shaded regions represent the 95%, 68%, and 5% credible regions for the data. The reported errors above the plot represent the 68% credible region on the mutant relative fitness marginal distribution. (D) Comparison between the ground truth fitness value from the logistic-growth simulation and the inferred fitness value. Gray error bars represent the 68% posterior credible region for the relative fitness values. (E) The empirical cumulative distribution function (ECDF) for the absolute z-score value of the ground truth parameter value within the inferred fitness posterior distribution.

266 **Fitness inference on multiple environments**

267 The fitness model in Equation 3 relates nuisance parameters such as the population mean  
268 fitness and the barcode frequencies to the relative fitness parameter we want to infer from  
269 the data. These dependencies imply that uncertainty on the estimates of these nuisance  
270 parameters influences the inference of the relevant parameters. For example, imagine a  
271 scenario where the neutral lineages data were incredibly noisy, leading to poor estimates of the  
272 population mean fitness values  $\bar{s}_T$ . Since the relative fitness of any non-neutral barcode  $s^{(m)}$  is  
273 determined with respect to these neutral barcodes, not accounting for the lack of precision in  
274 the value of the population mean fitness would result in misleading estimates of the accuracy  
275 with which we determine the value of the parameter we care about. Thus, propagating these  
276 sources of uncertainty in nuisance parameters is vital to generate an unbiased estimate of  
277 the relevant information we want to extract from the data. One of the benefits of Bayesian  
278 methods is the intrinsic error propagation embedded in the mathematical framework. For  
279 our previous example, the uncertainty on the value of the population mean fitness values is  
280 propagated to the relative fitness of a non-neutral barcode since we defined a joint posterior  
281 distribution over all parameters as fully expressed in Equation 16.

282 This natural error propagation can help us with the experimental design schematized in  
283 Figure 3(A). Here, rather than performing growth-dilution cycles in the same environment,  
284 the cells are diluted into a different environment. Thus, the uncertainty on the fitness estimate  
285 for the previous environment must be propagated to that of the next one. To validate the  
286 extension of our statistical model to this scenario, Figure 3(B) shows the trajectory of the log  
287 frequency ratios between adjacent time points. The different colored regions correspond to the  
288 different environments. For this simulation, the growth rate of Environment 2 was set to be,  
289 on average, half of the average growth rate in Environment 1. Equivalently, the growth rate  
290 in Environment 3 was set to be, on average, twice the average growth rate in Environment  
291 1. Figure 3(C-E) show the correspondence between the simulation ground truth and the  
292 inferred fitness values, where the error bars represent the 68% credible region. Figure 3(F)  
293 summarizes the performance of our inference pipeline by showing the empirical cumulative  
294 distribution functions for the absolute value of the ground truth fitness value z-score within  
295 the posterior distribution. This plot shows that, overall,  $\approx 75\%$  of inferred mean values fall  
296 within one standard deviation of the ground truth. For completeness, Figure 3(G) shows the  
297 posterior predictive checks for a few example barcodes.

298 **Accounting for experimental replicates via hierarchical models**

299 Our inference pipeline can be extended to account for multiple experimental replicates via  
300 Bayesian hierarchical models<sup>13</sup>. Briefly, when accounting for multiple repeated measurements  
301 of the same phenomena, there are two extreme cases one can use to perform the data analysis:  
302 On the one hand, we can treat each measurement as entirely independent, losing the power  
303 to utilize multiple measurements when trying to learn a single parameter. This can negatively  
304 impact the inference since, in principle, the value of our parameter of interest should not

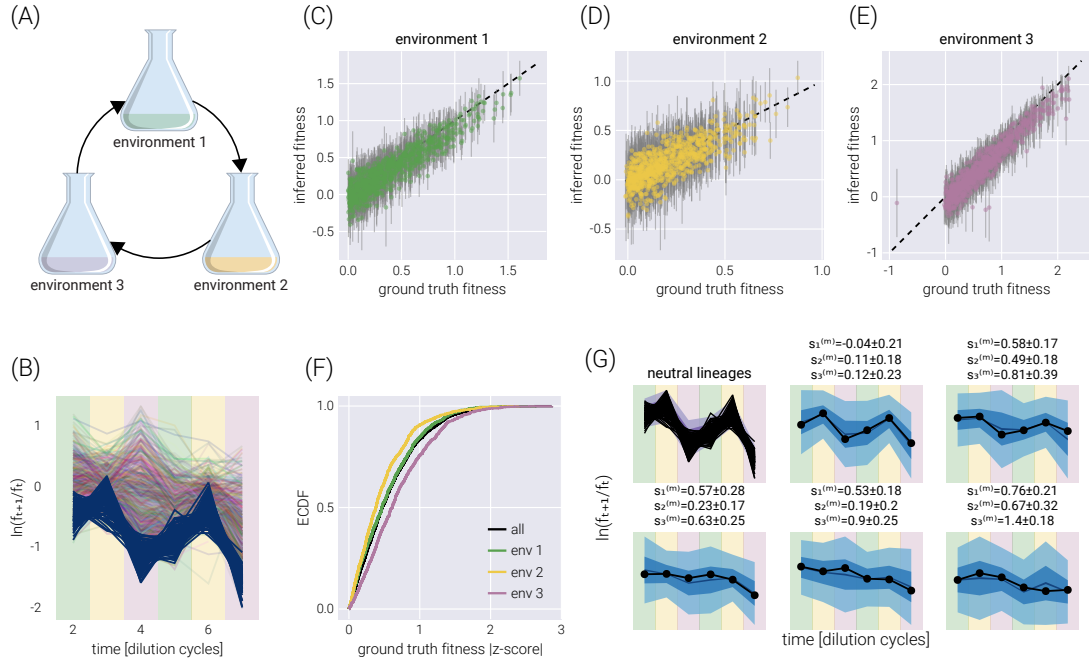


**Figure 3. Multi-environment fitness inference.** (A) Schematic of the simulated experimental design where growth-dilution cycles are performed into different environments for each cycle. (B) log frequency ratios between adjacent time points. Darker lines represent the neutral barcodes. The colors in the background demarcate the corresponding environment, matching colors in (A). Environment 2 is set to have, on average, half the growth rate of environment 1. Likewise, environment 3 is set to have, on average, twice the growth rate of environment 1. (C-E) Comparison between the ground truth fitness value from the logistic-growth simulation and the inferred fitness value for each environment. Gray error bars represent the 68% posterior credible region. (F) The empirical cumulative distribution function (ECDF) for the absolute z-score value of the ground truth parameter value within the inferred fitness posterior distribution for all fitness values (black line) and each environment individually (color lines). (G) Examples of the posterior predictive checks for all neutral lineages (upper left panel) and a subset of representative mutant lineages. Shaded regions surrounding the data represent the 95%, 68%, and 5% credible regions for the data. The reported errors above the plot represent the 68% credible region on the mutant relative fitness marginal distribution. Background colors match those of (A).

305 depend on the particular experimental replicate in question. However, this approach does  
306 not allow us to properly “combine” the uncertainties in both experiments when performing  
307 the inference. On the other hand, we can pool all data together and treat our different  
308 experiments as a single measurement with higher coverage. This loses the subtle differences  
309 due to biotic and abiotic batch effects, effectively halving the data that goes into our inference  
310 problem.

311 Hierarchical models present a middle ground between these extremes. First, hierarchical  
312 models rely on the definition of so-called *hyper-parameters*, that capture the parametric  
313 inference we are interested in—for this inference problem, we have a hyper-fitness value  
314  $\theta^{(m)}$  for each non-neutral barcode. Second, each experiment draws randomly from the  
315 distribution of this hyper-parameter, allowing for subtle variability between experiments to be  
316 accounted for—in the present inference pipeline, each experimental replicate gets assigned a  
317 *local* fitness value  $s_i^{(m)}$ , where the extra sub-index indicates the  $i$ -th experimental replicate.  
318 Conceptually, we can think of the local fitness for replicate  $i$  as being sampled from a  
319 distribution that depends on the value of the global hyper-fitness value, i.e.,  $s_i^{(m)} \sim \pi_{\theta^{(m)}}$ ,  
320 where the subindex  $\theta^{(m)}$  indicates the distribution’s parametric dependence on the hyper-  
321 fitness value. This way of interpreting the connection between the distribution  $\pi_{\theta^{(m)}}$  and  
322 the local fitness implies that a large replicate-to-replicate variability would lead to a broad  
323 hyper-fitness distribution—implying a large uncertainty when determining the parameter that  
324 characterizes the overall relative fitness. We point the reader to Section for the full definition  
325 of the hierarchical model used in this section. Importantly, as schematized in Figure 4(A),  
326 the influence between different experimental replicates runs both ways. First, the data from  
327 one experimental replicate ( $R_k^M$  in the diagram) informs all local fitness values via the global  
328 hyper-fitness (upper panel in Figure 4(A)). Second, the local fitness value is informed by the  
329 data from all experimental replicates via the same global hyper-fitness parameter (lower panel  
330 in Figure 4(A)).

331 To test the performance of this model, we simulated two experimental replicates with 1000  
332 unique barcodes (see Figure 4(B-C)) where we randomly sampled a ground truth hyper-fitness  
333 value  $\theta^{(m)}$  for each barcode. We sampled a variation from this hyper-fitness value for each  
334 experimental replicate  $s_i^{(m)}$  to capture experimental batch effects. Figure 4(D) shows the  
335 relationship between hyper-fitness and replicate fitness values for this simulation. The spread  
336 around the identity line represents the expected batch-to-batch variation. The posterior  
337 predictive checks examples in Figure 4(E) show that the hierarchical model can correctly fit  
338 the data for each experimental replicate. Furthermore, Figure 4(F-G) show a high correlation  
339 between the ground truth and the inferred fitness values. The empirical cumulative distribution  
340 functions shown in Figure 4(H-I) reveal that for  $\approx 75\%$  of the non-neutral barcodes, the  
341 ground truth hyper-fitness values fall within one standard deviation from the mean value in  
342 the posterior distributions.

343 As shown in Figure 5, the structure imposed by the hierarchical model schematized in  
344 Figure 4(A), where we explicitly account for the connection between experimental replicates  
345 can improve the quality of the inference. Inferred fitness values between experimental  
346 replicates exhibit a stronger degree of correlation in the hierarchical model (Figure 5(A))

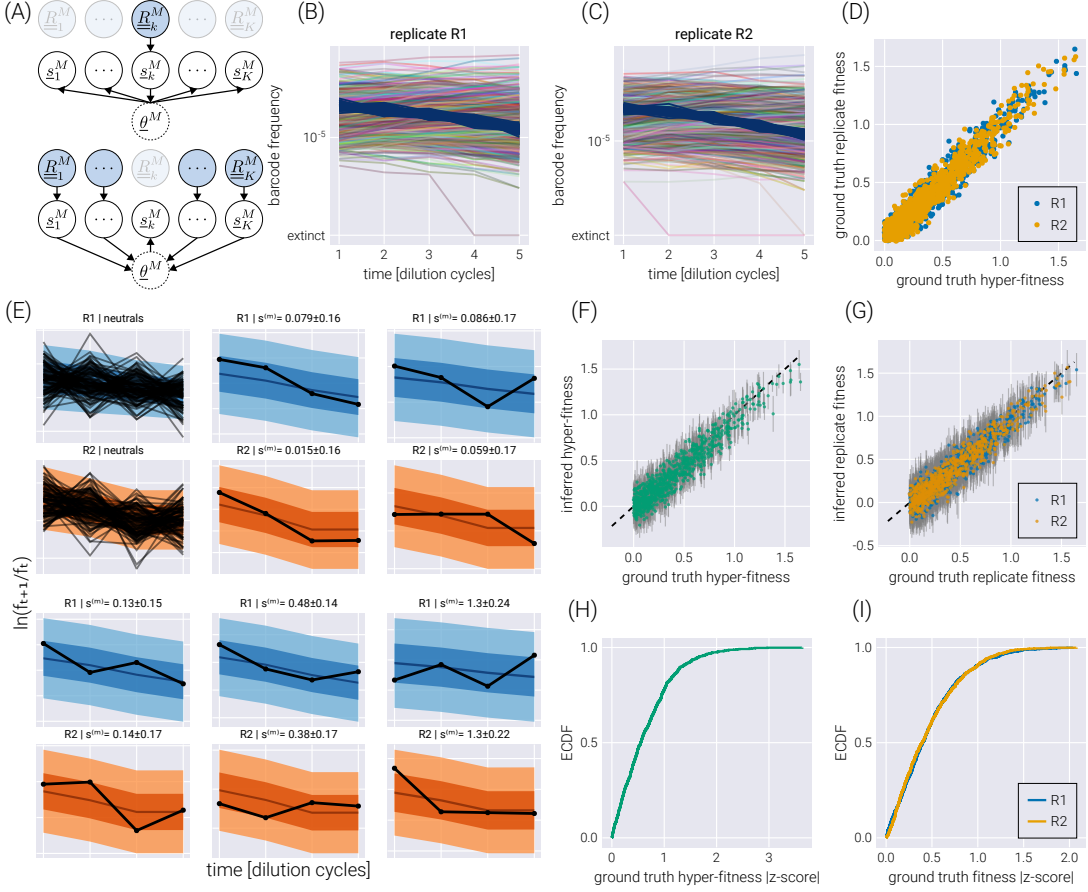


**Figure 4. Hierarchical model on experimental replicates.** (A) Schematic depiction of the interactions between local fitness values  $\underline{s}_k^M$  through the global hyper-fitness value  $\theta^M$  for  $K$  hypothetical experimental replicates. The upper diagram shows how the data from replicate  $k$  informs all local fitness values via the hyper-fitness parameter. The lower panel shows the reverse, where all other datasets inform the local fitness value. (B-C) Simulated replicate datasets with 900 barcodes of interest and 100 neutral lineages. (D) Comparison between the simulation ground truth hyper-fitness and each replicate ground truth fitness. The scatter between parameters captures experimental batch effects. (E) Examples of the posterior predictive checks for all neutral lineages (upper left panels) and a subset of representative mutant lineages. Shaded regions from light to dark represent the 95%, 68%, and 5% credible regions. (F-G) Comparison between the simulation's ground truth hyper-fitness (F) and replicate fitness (G) values and the inferred parameters. Gray error bars represent the 68% posterior credible region. (H-I) The empirical cumulative distribution function (ECDF) for the absolute z-score value of the ground truth parameter value within the inferred hyper-fitness posterior distribution (H) and replicate fitness (I).

347 compared to conducting inference on each replicate independently (Figure 5(B)). Moreover,  
348 when comparing the inferred hyper-fitness values—the objective parameter when performing  
349 multiple experimental measurements—the hierarchical model outperforms averaging the  
350 independent experimental replicates as shown in Figure 5(C) and (D).

351 **Accounting for multiple barcodes per genotype via hierarchical models**

352 Hierarchical models can also capture another experimental design in which multiple barcodes  
353 map to the same or an equivalent genotype. As we will show, this many-to-one mapping  
354 can improve the inference compared to the extreme cases of inferring the fitness of each  
355 barcode independently or pooling the data of all barcodes mapping to a single genotype. As  
356 schematized in Figure 6(A), a small modification of the base model allows us to map the  
357 structure of our original model to that of a hierarchical model with a fitness hyperparameter  
358 vector  $\theta^G$ , where  $G$  is the number of genotypes in the dataset.

359 Figure 6(B) shows a single experimental replicate in which 90 genotypes were assigned  
360 a random number of barcodes (a multinomial distribution with a mean of ten barcodes  
361 per genotype) for a total of 900 non-neutral barcodes. To assess the performance of the  
362 hierarchical model proposed in Figure 6(A), we performed inference using this hierarchical  
363 model, as well as the two extreme cases of ignoring the connection between the barcodes  
364 belonging to the same genotype—equivalent to performing inference using the model presented  
365 in Figure 2(A) over the barcodes—or pooling the data of all barcodes belonging to the same  
366 genotype into a single count—equivalent to performing inference using the model presented  
367 in Figure 2(A) over the pooled barcodes. Figure 6(C-D) shows the comparison between  
368 the simulation ground truth and the inferred values for these three cases. Not only do the  
369 hierarchical model results show higher degrees of correlation with the ground truth, but the  
370 error bars (representing the 68% credible regions) are smaller, meaning that the uncertainty  
371 in the estimate of the parameter we care about decreases when using the hierarchical model.  
372 The improvement in the prediction can be seen in Figure 6(F) where the empirical cumulative  
373 distribution function of the absolute difference between the mean inferred value and the  
374 simulation ground truth is shown for all three inference models. The hierarchical model's  
375 curve ascends more rapidly, showing that, in general, the inferred values are closer to the  
376 ground truth. For completeness, Figure 6(G) shows some examples of how the hierarchical  
377 model can capture the raw log-frequency count observations.

378 **Discussion**

379 Experimental evolution of microbial systems has dramatically advanced our understanding  
380 of the basic principles of biological evolution<sup>14</sup>. From questions related to the optimal  
381 fine-tuning of gene expression programs<sup>15</sup>, to the dimensionality, geometry, and accessibility  
382 of the adaptive fitness landscape explored by these rapidly adapting populations<sup>4,16</sup>, to the  
383 emergence of eco-evolutionary dynamics in a long-term evolution experiment<sup>17</sup>; for all of

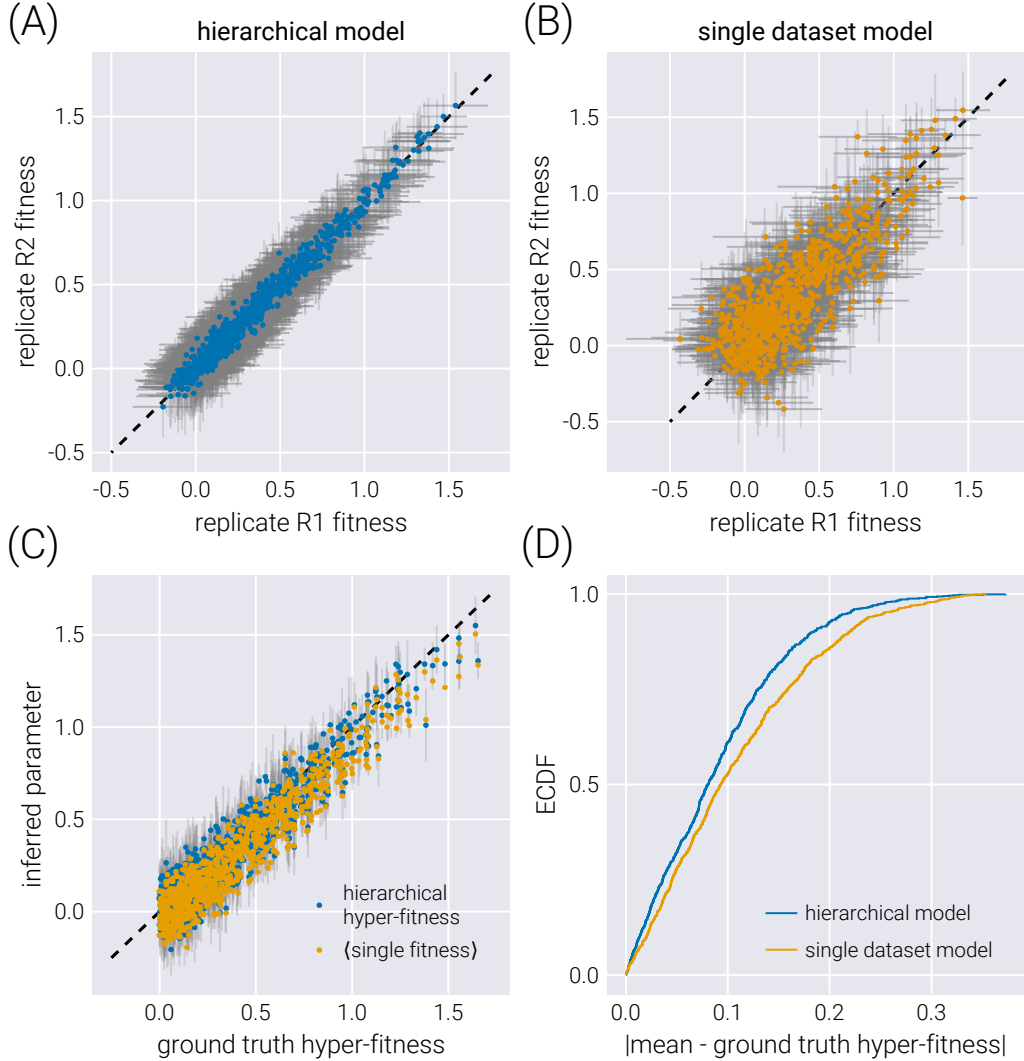


**Figure 5. Comparison between hierarchical model and single dataset model.** (A-B) comparison of inferred fitness values between experimental replicates when fitting a hierarchical model (A) or independently fitting each dataset (B). Gray error bars represent the 68% credible regions. (C) Comparison between the ground truth hyper-fitness value and the inferred parameters. The blue dots show the inferred hyper-fitness values when assuming a hierarchical model. Gray error bars show the 68% credible region for this inference. The yellow dots show the average of the mean inferred fitness values for the two experimental replicates. No error bars are shown for these, as it is inappropriate to compute one with two data points per non-neutral barcode. (D) Empirical cumulative distribution function (ECDF) of the absolute difference between the inferred mean and the ground truth hyper-fitness.

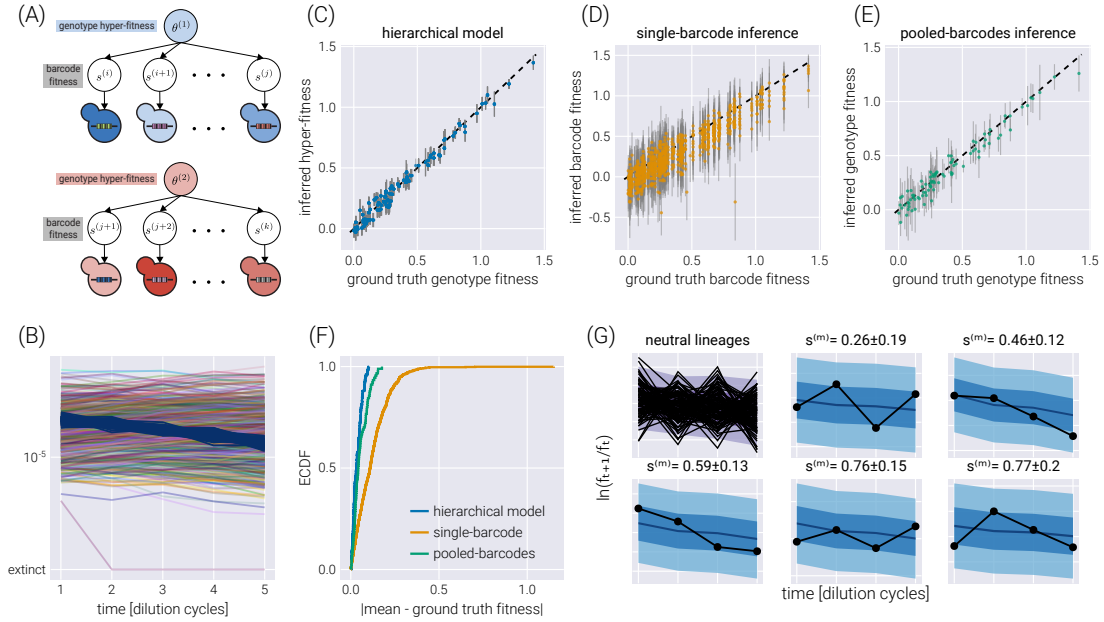


**Figure 6. Hierarchical model for multiple barcodes per genotype.** (A) Schematic depiction of the hierarchical structure for multiple barcodes mapping to a single genotype. A set of barcodes mapping to an equivalent genotype map to “local” fitness values  $s^{(b)}$  that are connected via a hyper-fitness parameter for the genotype  $\theta^{(g)}$ . (B) Simulated dataset with 100 neutral lineages and 900 barcodes of interest distributed among 90 genotypes. (C-E) Comparison between the inferred and ground truth fitness values for a hierarchical model (C), a model where each barcode is inferred independently (D), and a model where barcodes mapping to the same genotype are pooled together (E). Gray error bars represent the 68% credible regions. (F) Empirical cumulative distribution function (ECDF) of the absolute difference between the inferred mean and the ground truth fitness values for all three models. (G) Examples of the posterior predictive checks for all neutral lineages (upper left panels) and a subset of representative mutant lineages. Shaded regions from light to dark represent the 95%, 68%, and 5% credible regions.

384 these and other cases, the microbial experimental platform combined with high-throughput  
385 sequencing has been essential to tackling these questions with empirical data. This exciting  
386 research area promises to improve as new culturing technologies<sup>18</sup> as well as more complex  
387 lineage barcoding schemes<sup>2,19</sup>, are adopted.

388 For this data-heavy field, properly accounting for the uncertainty in parameters inferred from  
389 experiments is vital to ensure the conclusions drawn are reliable. Bayesian statistics presents  
390 a principled way to quantify this uncertainty systematically<sup>20</sup>. Moreover, Bayesian analysis  
391 offers a more natural way to interpret the role that probability theory plays when performing  
392 data analysis compared to the often-misinterpreted frequentist methods<sup>21</sup>. Nevertheless, the  
393 technical challenges associated with Bayesian analysis has limited its application. This is set  
394 to change as recognition of the misuse of frequentist concepts such as the p-value is receiving  
395 more attention<sup>22</sup>. Moreover, advances in numerical methods such as Hamiltonian Monte  
396 Carlo<sup>6</sup> and variational inference<sup>7</sup> allows for complex Bayesian models to be fit to empirical  
397 data.

398 In this paper, we present a computational pipeline to analyze lineage-tracking time-series data  
399 for massive-parallel competition assays. More specifically, we fit a Bayesian model to infer  
400 the fitness of multiple genotypes relative to a reference<sup>3,4</sup>. The proposed model accounts for  
401 multiple sources of uncertainty with proper error propagation intrinsic to Bayesian methods.  
402 To scale the inference pipeline to large datasets with > 10,000 barcodes, we use the ADVI  
403 algorithm<sup>7</sup> to fit a variational posterior distribution. The main difference between our method  
404 and previous inference pipelines, such as Li et al. [23], is that the present analysis provides  
405 interpretable errors on the inferred fitness values. The reported uncertainty intervals—known  
406 as credible regions—can be formally interpreted as capturing the corresponding probability  
407 mass of finding the true value of the parameter given the model, the prior information, and  
408 the data. Furthermore, minor modifications to the structure of the statistical model presented  
409 in this work allow for the analysis of different experimental designs, such as growth-dilution  
410 cycles in different environments, joint analysis of multiple experimental replicates of the same  
411 experiment via hierarchical models, and a hierarchical model for multiple barcodes mapping  
412 to equivalent genotypes. We validate our analysis pipeline on simulated datasets with known  
413 ground truth, showing that the model fits the data adequately, capturing the ground truth  
414 parameters within the posterior distribution.

415 It is important to highlight some of the consequences of the general experimental design and  
416 the implicit assumptions within the proposed statistical model to analyze the resulting data.  
417 First, the composition of the population is such that the initial fraction of the population  
418 occupied by the barcoded genotypes is small—usually >90% of the initial population is  
419 the non-labeled reference strain. This constraint is important as the fitness model used  
420 to fit the time series data assumes that the tracked frequencies are  $\ll 1$ . Second, when  
421 computing log frequency ratios, we can run into the issue of dividing by zero. This is a  
422 common problem when dealing with molecular count data<sup>24</sup>. Our model gets around this issue  
423 by assuming that the frequency of any barcode cannot be, but still can get arbitrarily close  
424 to, zero. Therefore, we implicitly assume that no lineage goes extinct during the experiment.  
425 Moreover, the statistical model directly accounts for the uncertainty associated with having

426 zero barcode counts, increasing the corresponding uncertainty. Third, the models presented  
427 in this paper require the existence of a labeled sub-population of barcoded reference strains.  
428 These barcodes help determine the fitness baseline, as every fitness is quantified with respect  
429 to this reference genotype. This experimental design constraint facilitates the inference of  
430 the population mean fitness since most of the culture—the unlabeled reference genotype—is  
431 not tracked. Finally, the presented statistical model assumes that relative fitness is solely a  
432 constant of the environment and the genotype. Future directions of this work could extend  
433 the fitness model to properly analyze data with time-varying or frequency-dependent fitness  
434 values.

435 In total, the statistical model presented in this work and the software package accompanying  
436 the paper allow for a principled way of quantifying the accuracy with which we can extract  
437 relevant parametric information from large-scale multiplexed fitness competition assays. Fur-  
438 thermore, the implementation of Bayesian models and their fitting via automatic differentiation  
439 approaches opens the gate to extend this type of formal analysis to the data-rich literature in  
440 experimental evolution and other high-throughput technologies applications.

## 441 Acknowledgements

442 We would like to thank Griffin Chure and Michael Betancourt for their helpful advice and  
443 discussion. We would like to thank Karna Gowda, Spencer Farrell, and Shaili Mathur for  
444 critical observations on the manuscript. This work was supported by the NIH/NIGMS,  
445 Genomics of rapid adaptation in the lab and in the wild R35GM11816506 (MIRA grant),  
446 the NIH, Unravelling mechanisms of tumor suppression in lung cancer R01CA23434903,  
447 the NIH (PQ4), Quantitative and multiplexed analysis of gene function in cancer in vivo  
448 R01CA23125303, the NIH, Genetic Determinants of Tumor Growth and Drug Sensitivity  
449 in EGFR Mutant Lung Cancer R01CA263715, the NIH, Dissecting the interplay between  
450 aging, genotype, and the microenvironment in lung cancer U01AG077922, the NIH, Genetic  
451 dissection of oncogenic Kras signaling R01CA230025, and the CZ Biohub investigator program.  
452 MRM was supported by the Schmidt Science Fellowship. MM was supported by The National  
453 Science Foundation-Simons Center for Quantitative Biology at Northwestern University and  
454 the Simons Foundation grant 597491. MM is a Simons Investigator. DP is a CZ Biohub  
455 investigator.

## 456 References

- 457 <sup>1</sup>S. F. Levy, J. R. Blundell, S. Venkataram, D. A. Petrov, D. S. Fisher, and G. Sherlock,  
458 “Quantitative evolutionary dynamics using high-resolution lineage tracking”, *Nature* **519**,  
459 [181–186 \(2015\)](#).
- 460 <sup>2</sup>A. N. Nguyen Ba, I. Cvijović, J. I. Rojas Echenique, K. R. Lawrence, A. Rego-Costa, X. Liu,  
461 S. F. Levy, and M. M. Desai, “High-resolution lineage tracking reveals travelling wave of  
462 adaptation in laboratory yeast”, *Nature* **575**, [494–499 \(2019\)](#).

- 463   <sup>3</sup>J. A. Ascensao, K. M. Wetmore, B. H. Good, A. P. Arkin, and O. Hallatschek, "Quantifying  
 464   the local adaptive landscape of a nascent bacterial community", *Nature Communications*  
 465   **14**, 248 (2023).
- 466   <sup>4</sup>G. Kinsler, K. Geiler-Samerotte, and D. A. Petrov, "Fitness variation across subtle environ-  
 467   mental perturbations reveals local modularity and global pleiotropy of adaptation", *eLife* **9**,  
 468   1–52 (2020).
- 469   <sup>5</sup>S. R. Eddy, "What is Bayesian statistics?", *Nature Biotechnology* **22**, 1177–1178 (2004).
- 470   <sup>6</sup>M. Betancourt, "A Conceptual Introduction to Hamiltonian Monte Carlo", ArXiv (2017).
- 471   <sup>7</sup>A. Kucukelbir, D. Tran, R. Ranganath, A. Gelman, and D. M. Blei, *Automatic Differentiation  
 472   Variational Inference*, (Mar. 2, 2016) (visited on 07/07/2023), preprint.
- 473   <sup>8</sup>B. Efron, "Bayes' Theorem in the 21st Century", *Science* **340**, 1177–1178 (2013).
- 474   <sup>9</sup>D. P. Kingma and M. Welling, *Auto-Encoding Variational Bayes*, (May 1, 2014) <http://arxiv.org/abs/1312.6114> (visited on 11/21/2022), preprint.
- 476   <sup>10</sup>S. Gottwald and D. A. Braun, "The two kinds of free energy and the Bayesian revolution",  
 477   *PLOS Computational Biology* **16**, e1008420 (2020).
- 478   <sup>11</sup>H. Ge, K. Xu, and Z. Ghahramani, "Turing: A Language for Flexible Probabilistic Inference",  
 479   in *Proceedings of the Twenty-First International Conference on Artificial Intelligence and  
 480   Statistics* (Mar. 31, 2018), pp. 1682–1690.
- 481   <sup>12</sup>R. D. Morey, R. Hoekstra, J. N. Rouder, M. D. Lee, and E.-J. Wagenmakers, "The fallacy  
 482   of placing confidence in confidence intervals", *Psychonomic Bulletin & Review* **23**, 103–123  
 483   (2016).
- 484   <sup>13</sup>M. J. Betancourt and M. Girolami, *Hamiltonian Monte Carlo for Hierarchical Models*,  
 485   (Dec. 3, 2013) <http://arxiv.org/abs/1312.0906> (visited on 07/20/2023), preprint.
- 486   <sup>14</sup>E. Kussell, "Evolution in Microbes", *Annu. Rev. Biophys* **42**, 493–514 (2013).
- 487   <sup>15</sup>E. Dekel and U. Alon, "Optimality and evolutionary tuning of the expression level of a  
 488   protein", *Nature* **436**, 588–592 (2005).
- 489   <sup>16</sup>T. Maeda, J. Iwasawa, H. Kotani, N. Sakata, M. Kawada, T. Horinouchi, A. Sakai, K.  
 490   Tanabe, and C. Furusawa, "High-throughput laboratory evolution reveals evolutionary  
 491   constraints in *Escherichia coli*", *Nature Communications* **11**, 5970 (2020).
- 492   <sup>17</sup>B. H. Good, M. J. McDonald, J. E. Barrick, R. E. Lenski, and M. M. Desai, "The dynamics  
 493   of molecular evolution over 60,000 generations", *Nature*, 10.1038/nature24287 (2017).
- 494   <sup>18</sup>T. Jagdish and A. N. Nguyen Ba, "Microbial experimental evolution in a massively multi-  
 495   plexed and high-throughput era", *Current Opinion in Genetics & Development* **75**, 101943  
 496   (2022).
- 497   <sup>19</sup>D. Yang et al., "Lineage tracing reveals the phylodynamics, plasticity, and paths of tumor  
 498   evolution", *Cell* **185**, 1905–1923.e25 (2022).
- 499   <sup>20</sup>A. Gelman and C. R. Shalizi, "Philosophy and the practice of Bayesian statistics", *Statistics  
 500   math.ST*, 36 (2010).

- 501   <sup>21</sup>J. VanderPlas, “Frequentism and Bayesianism: A Python-driven Primer”, [ArXiv](#), 1–9 (2014).
- 502   <sup>22</sup>R. Nuzzo, “Statistical errors”, *Nature* **506** (2014).
- 503   <sup>23</sup>F. Li, J. Tarkington, and G. Sherlock, “Fit-Seq2.0: An Improved Software for High-
- 504   Throughput Fitness Measurements Using Pooled Competition Assays”, [Journal of Molecular](#)
- 505   [Evolution](#), [10.1007/s00239-023-10098-0](#) (2023).
- 506   <sup>24</sup>D. R. Lovell, X.-Y. Chua, and A. McGrath, “Counts: an outstanding challenge for log-
- 507   ratio analysis of compositional data in the molecular biosciences”, [NAR Genomics and](#)
- 508   [Bioinformatics](#) **2**, lqaa040 (2020).

509 **Supplementary Materials**

510 **Table of contents**

511	<b>Supplementary Materials</b>	<b>22</b>
512	Primer on Variational Inference . . . . .	22
513	ADVI algorithm . . . . .	26
514	Defining the Bayesian model . . . . .	27
515	Frequency uncertainty $\pi(\underline{F}   \underline{R})$ . . . . .	27
516	Population mean fitness uncertainty $\pi(\bar{s}_T   \underline{F}, \underline{R})$ . . . . .	29
517	Mutant relative fitness uncertainty $\pi(\underline{s}^M   \bar{s}_T, \underline{F}, \underline{R})$ . . . . .	33
518	Hierarchical models for multiple experimental replicates . . . . .	35
519	Defining prior probabilities . . . . .	38
520	Posterior predictive checks . . . . .	40
521	Logistic growth simulation . . . . .	41

522 **Primer on Variational Inference**

523 In this section, we will briefly introduce the idea behind variational inference. Recall that  
524 any Bayesian inference problem deals with the joint distribution between observations  $\underline{x}$  and  
525 unobserved latent variables  $\underline{\theta}$ . This joint distribution can be written as the product of a  
526 distribution of the observations  $\underline{x}$  conditioned on the  $\underline{\theta}$  and the marginal distribution of these  
527 latent variables, i.e.,

$$\pi(\underline{x}, \underline{\theta}) = \pi(\underline{x} | \underline{\theta})\pi(\underline{\theta}). \quad (\text{S1})$$

528 A Bayesian inference pipeline's objective is to compute the latent variables' posterior probability  
529 given a set of observations. This computation is equivalent to updating our prior beliefs  
530 about the set of values that the latent variables take after taking in new data. We write this  
531 as Bayes theorem

$$\pi(\underline{\theta} | \underline{x}) = \frac{\pi(\underline{x} | \underline{\theta})\pi(\underline{\theta})}{\pi(\underline{x})}. \quad (\text{S2})$$

532 The main technical challenge for working with Equation S2 comes from the computation  
533 of the denominator, also known as the *evidence* or the *marginalized likelihood*. The reason  
534 computing this term is challenging is because it involves a (potentially) high-dimensional  
535 integral of the form

$$\pi(\underline{x}) = \int \cdots \int d^K \underline{\theta} \pi(\underline{x}, \underline{\theta}) = \int \cdots \int d^K \underline{\theta} \pi(\underline{x} | \underline{\theta})\pi(\underline{\theta}), \quad (\text{S3})$$

536 where  $K$  is the dimensionality of the  $\underline{\theta}$  vector. Here, the integrals are taken over the support—  
537 the set of values valid for the distribution—of  $\pi(\underline{\theta})$ . However, only a few selected distributions  
538 have a closed analytical form; thus, in most cases Equation S3 must be solved numerically.

539 Integration in high-dimensional spaces can be computationally extremely challenging. For a  
 540 naive numerical quadrature procedure, integrating over a grid of values for each dimension of  
 541  $\theta$  comes with an exponential explosion of the number of required grid point evaluations, most  
 542 of which do not contribute significantly to the integration. To gain visual intuition about  
 543 this challenge, imagine integrating the function depicted in Figure S1. If the location of the  
 544 high-density region (dark peak) is unknown, numerical quadrature requires many grid points  
 545 to ensure we capture this peak. However, most of the numerical evaluations of the function on  
 546 the grid points do not contribute significantly to the integral. Therefore, our computational  
 547 resources are wasted on insignificant evaluations. This only gets worse as the number of  
 548 dimensions increases since the number of grid point evaluation scales exponentially.

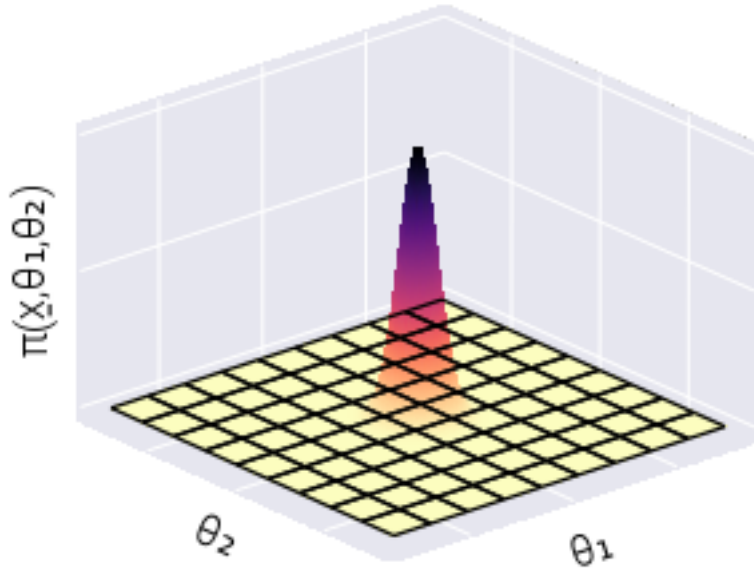


**Figure S1. High-dimensional numerical quadrature does not scale with dimensionality.**

Schematic depiction of the problem with naive numerical quadrature to integrate over an unknown density. While the density is concentrated on the dark peak, most of the evaluations over the  $x_1 - x_2$  grid do not contribute to the value of the integral

549 Modern Markov Chain Monte Carlo algorithms, such as Hamiltonian Monte Carlo, can  
 550 efficiently perform this high-dimensional integration by utilizing gradient information from  
 551 the target density Betancourt [6]. Nevertheless, these sampling-based methods become  
 552 prohibitively slow for the number of dimensions our present inference problem presents. Thus,  
 553 there is a need to find scalable methods for the inference problem in Equation S2.

554 Variational inference circumvents these technical challenges by proposing an approximate

555 solution to the problem. Instead of working with the posterior distribution in its full glory  
 556  $\pi(\underline{\theta} | \underline{x})$ , let us propose an approximate posterior distribution  $q_\phi$  that belongs to a distribution  
 557 family fully parametrized by  $\phi$ . For example, let us say that the distribution  $q_\phi$  belongs  
 558 to the family of multivariate Normal distributions such that  $\phi = (\underline{\mu}, \underline{\Sigma})$ , where  $\underline{\mu}$  is the  
 559 vector of means and  $\underline{\Sigma}$  is the covariance matrix. If we replace  $\pi$  by  $q_\phi$ , we want  $q_\phi$  to  
 560 resemble the original posterior as much as possible. Mathematically, this can be expressed as  
 561 minimizing a “*distance metric*”—the Kullback-Leibler (KL) divergence, for example—between  
 562 the distributions. Note that we use quotation marks because, formally, the KL divergence is  
 563 not a distance metric since it is not symmetric. Nevertheless, the variational objective is set  
 564 to find a distribution  $q_\phi^*$  such that

$$q_\phi^*(\underline{\theta}) = \min_{\phi} D_{KL}(q_\phi(\underline{\theta}) || \pi(\underline{\theta} | \underline{x})), \quad (\text{S4})$$

565 where  $D_{KL}$  is the KL divergence. Furthermore, we highlight that the KL divergence is a  
 566 strictly positive number, i.e.,

$$D_{KL}(q_\phi(\underline{\theta}) || \pi(\underline{\theta} | \underline{x})) \geq 0, \quad (\text{S5})$$

567 as this property will become important later on.

568 At first sight, Equation S4 does not improve the situation but only introduces further technical  
 569 complications. After all, the definition of the KL divergence

$$D_{KL}(q_\phi(\underline{\theta}) || \pi(\underline{\theta} | \underline{x})) \equiv \int \cdots \int d^K \underline{\theta} q_\phi(\underline{\theta}) \ln \frac{q_\phi(\underline{\theta})}{\pi(\underline{\theta} | \underline{x})}, \quad (\text{S6})$$

570 includes the posterior distribution  $\pi(\underline{\theta} | \underline{x})$  we are trying to get around. However, let us  
 571 manipulate Equation S6 to beat it to a more reasonable form. First, we can use the properties  
 572 of the logarithms to write

$$D_{KL}(q_\phi(\underline{\theta}) || \pi(\underline{\theta} | \underline{x})) = \int d^K \underline{\theta} q_\phi(\underline{\theta}) \ln q_\phi(\underline{\theta}) - \int d^K \underline{\theta} q_\phi(\underline{\theta}) \ln \pi(\underline{\theta} | \underline{x}), \quad (\text{S7})$$

573 where, for convenience, we write a single integration sign ( $d^K \underline{\theta}$  still represents a multi-  
 574 dimensional differential). For the second term in Equation S7, we can substitute the term  
 575 inside the logarithm using Equation S2. This results in

$$\begin{aligned} D_{KL}(q_\phi(\underline{\theta}) || \pi(\underline{\theta} | \underline{x})) &= \int d^K \underline{\theta} q_\phi(\underline{\theta}) \ln q_\phi(\underline{\theta}) \\ &\quad - \int d^K \underline{\theta} q_\phi(\underline{\theta}) \ln \left( \frac{\pi(\underline{x} | \underline{\theta}) \pi(\underline{\theta})}{\pi(\underline{x})} \right). \end{aligned} \quad (\text{S8})$$

576 Again, using the properties of logarithms, we can split Equation S8, obtaining

$$\begin{aligned} D_{KL}(q_\phi(\underline{\theta}) || \pi(\underline{\theta} | \underline{x})) &= \int d^K \underline{\theta} q_\phi(\underline{\theta}) \ln q_\phi(\underline{\theta}) \\ &\quad - \int d^K \underline{\theta} q_\phi(\underline{\theta}) \ln \pi(\underline{x} | \underline{\theta}) \\ &\quad - \int d^K \underline{\theta} q_\phi(\underline{\theta}) \ln \pi(\underline{\theta}) \\ &\quad + \int d^K \underline{\theta} q_\phi(\underline{\theta}) \ln \pi(\underline{x}). \end{aligned} \quad (\text{S9})$$

577 It is convenient to write Equation S9 as

$$\begin{aligned} D_{KL}(q_\phi(\underline{\theta}) || \pi(\underline{\theta} | \underline{x})) &= \int d^K \underline{\theta} q_\phi(\underline{\theta}) \ln \frac{q_\phi(\underline{\theta})}{\pi(\underline{\theta})} \\ &\quad - \int d^K \underline{\theta} q_\phi(\underline{\theta}) \ln \pi(\underline{x} | \underline{\theta}) \\ &\quad + \ln \pi(\underline{x}) \int d^K \underline{\theta} q_\phi(\underline{\theta}), \end{aligned} \quad (\text{S10})$$

578 where for the last term, we can take  $\ln \pi(\underline{x})$  out of the integral since it does not depend on  
579  $\underline{\theta}$ . Lastly, we utilize two properties:

580 1. The proposed approximate distribution must be normalized, i.e.,

$$\int d^K \underline{\theta} q_\phi(\underline{\theta}) = 1. \quad (\text{S11})$$

581 2. The law of the unconscious statistician (LOTUS) establishes that for any probability  
582 density function, it must be true that

$$\int d^K \underline{\theta} q_\phi(\underline{\theta}) f(\underline{\theta}) = \langle f(\underline{\theta}) \rangle_{q_\phi}, \quad (\text{S12})$$

583 where  $\langle \cdot \rangle_{q_\phi}$  is the expected value over the  $q_\phi$  distribution.

584 Using these two properties, the positivity constraint on the KL divergence in Equation S5,  
585 and the definition of the KL divergence in Equation S6 we can rewrite Equation S10 as

$$D_{KL}(q_\phi(\underline{\theta}) || \pi(\underline{\theta})) - \langle \ln \pi(\underline{x} | \underline{\theta}) \rangle_{q_\phi} \geq -\ln \pi(\underline{x}). \quad (\text{S13})$$

586 Multiplying by a minus one, we have the functional form of the so-called evidence lower  
587 bound (ELBO) Kingma and Welling [9],

$$\underbrace{\ln \pi(\underline{x})}_{\text{log evidence}} \geq \underbrace{\langle \ln \pi(\underline{x} | \underline{\theta}) \rangle_{q_\phi} - D_{KL}(q_\phi(\underline{\theta}) || \pi(\underline{\theta}))}_{\text{ELBO}}. \quad (\text{S14})$$

588 Let us recapitulate where we are. We started by presenting the challenge of working with  
589 Bayes' theorem, as it requires a high-dimensional integral of the form in Equation S3. As an  
590 alternative, variational inference posits to approximate the posterior distribution  $\pi(\underline{\theta} | \underline{x})$  with  
591 a parametric distribution  $q_\phi(\underline{\theta})$ . By minimizing the KL divergence between these distributions,  
592 we arrive at the result in Equation S14, where the left-hand side—the log marginalized  
593 likelihood or log evidence—we cannot compute for technical/computational reasons. However,  
594 the right-hand side is composed of things we can easily evaluate. We can easily evaluate  
595 the log-likelihood  $\ln \pi(\underline{x} | \underline{\theta})$  and the KL divergence between our proposed approximate  
596 distribution  $q_\phi(\underline{\theta})$  and the prior distribution  $\pi(\underline{\theta})$ . Moreover, we can compute the gradients of  
597 these functions with respect to the parameters of our proposed distribution. This last point  
598 implies that we can change the parameters of the proposed distribution to maximize the

599 ELBO. And, although we cannot compute the left-hand side of Equation S14, we know that  
600 however large we make the ELBO, it will always be smaller than (or equal) the log-marginal  
601 likelihood. Therefore, the larger we can make the ELBO by modifying the parameters  $\phi$ , the  
602 closer it gets to the log-marginal likelihood, and, as a consequence, the better our proposed  
603 distribution  $q_\phi(\underline{\theta})$  gets to the true posterior distribution  $\pi(\underline{\theta} | \underline{x})$ .

604 In this sense, variational inference turns the intractable numerical integration problem to an  
605 optimization routine, for which there are several algorithms available.

## 606 ADVI algorithm

607 To maximize the right-hand side of Equation S14, the Automatic Differentiation Variational  
608 Inference (ADVI) algorithm developed in<sup>7</sup> takes advantage of advances in probabilistic  
609 programming languages to generate a robust method to perform this optimization. Without  
610 going into the details of the algorithm implementation, for our purposes, it suffices to say  
611 that we define our joint distribution  $\pi(\underline{\theta}, \underline{x})$  as the product defined in Equation S1. ADVI  
612 then proposes an approximate variational distribution  $q_\phi$  that can either be a multivariate  
613 Normal distribution with a diagonal covariance matrix, i.e.,

$$\phi = (\underline{\mu}, \underline{\underline{D}}), \quad (\text{S15})$$

614 where  $\underline{\underline{D}}$  is the identity matrix, with the diagonal elements given by the vector of variances  
615  $\underline{\sigma}^2$  for each variable or a full-rank multivariate Normal distribution

$$\phi = (\underline{\mu}, \underline{\Sigma}). \quad (\text{S16})$$

616 Then, the parameters are initialized in some value  $\phi_o$ . These parameters are iteratively  
617 updated by computing the gradient of the ELBO (right-hand side of Equation S14), hereafter  
618 defined as  $\mathcal{L}$ , with respect to the parameters,

$$\nabla_\phi \mathcal{L} = \nabla_{\underline{\mu}} \mathcal{L} + \nabla_{\underline{\sigma}} \mathcal{L}, \quad (\text{S17})$$

619 and then computing

$$\phi_{t+1} = \phi_t + \eta \nabla_\phi \mathcal{L},$$

620 where  $\eta$  defines the step size.

621 This short explanation behind the ADVI algorithm is intended only to gain intuition on  
622 how the optimal variational distribution  $q_\phi$  be computed. There are many nuances in the  
623 implementation of the ADVI algorithm. We invite the reader to look at the original reference  
624 for further details.

625 **Defining the Bayesian model**

626 In the main text, we specify the inference problem we must solve as being of the form

$$\pi(\underline{s}^M, \bar{s}_T, \underline{F} | \underline{R}) \propto \pi(\underline{R} | \underline{s}^M, \bar{s}_T, \underline{F}) \pi(\underline{s}^M, \bar{s}_T, \underline{F}). \quad (\text{S18})$$

627 Here, we briefly define the missing nuisance parameters. Let

$$\bar{s}_T = (\bar{s}_1, \bar{s}_2, \dots, \bar{s}_{T-1})^\dagger, \quad (\text{S19})$$

628 be the vector containing the  $T - 1$  population mean fitness we compute from the  $T$  time  
629 points where measurements were taken. We have  $T - 1$  since the value of any  $\bar{s}_t$  requires  
630 cycle numbers  $t$  and  $t + 1$ . Furthermore, let the matrix  $\underline{F}$  be a  $T \times B$  matrix containing all  
631 frequency values. As with Equation 12 in the main text, we can split  $\underline{F}$  into two matrices of  
632 the form

$$\underline{F} = \begin{bmatrix} \underline{F}^N & \underline{F}^M \end{bmatrix}, \quad (\text{S20})$$

633 to separate the corresponding neutral and non-neutral barcode frequencies.

634 Let us now define each of the terms in Equation 18 described in Section of the main text.  
635 The following sections will specify the functional form each of these terms takes.

636 **Frequency uncertainty**  $\pi(\underline{F} | \underline{R})$

637 We begin with the probability of the frequency values given the raw barcode reads. The first  
638 assumption is that the inference of the frequency values for time  $t$  is independent of any other  
639 time. Therefore, we can write the joint probability distribution as a product of independent  
640 distributions of the form

$$\pi(\underline{F} | \underline{R}) = \prod_{t=1}^T \pi(\underline{f}_t | \underline{r}_t), \quad (\text{S21})$$

641 where  $\underline{f}_t$  and  $\underline{r}_t$  are the  $t$ -th row of the matrix containing all of the measurements for time  $t$ .  
642 We imagine that when the barcode reads are obtained via sequencing, the quantified number  
643 of reads is a Poisson sample from the “true” underlying number of barcodes within the pool.  
644 This translates to assuming that the number of reads for each barcode at any time point  $r_t^{(b)}$   
645 is an independent Poisson random variable, i.e.,

$$r_t^{(b)} \sim \text{Poiss}(\lambda_t^{(b)}), \quad (\text{S22})$$

646 where the symbol “~” is read “distributed as.” Furthermore, for a Poisson distribution, we  
647 have that

$$\lambda_t^{(b)} = \langle r_t^{(b)} \rangle = \left\langle \left( r_t^{(b)} - \langle r_t^{(b)} \rangle \right)^2 \right\rangle, \quad (\text{S23})$$

648 where  $\langle \cdot \rangle$  is the expected value. In other words the Poisson parameter is equal to the mean  
649 and variance of the distribution. The Poisson distribution has the convenient property that

650 for two Poisson distributed random variables  $X \sim \text{Poiss}(\lambda_x)$  and  $Y \sim \text{Poiss}(\lambda_y)$ , we have  
651 that

$$Z \equiv X + Y \sim \text{Poiss}(\lambda_x + \lambda_y). \quad (\text{S24})$$

652 This additivity allows us to write the total number of reads at time  $t$   $n_t$  also as a Poisson-  
653 distributed random variable of the form

$$n_t \sim \text{Poiss} \left( \sum_{b=1}^B \lambda_t^{(b)} \right), \quad (\text{S25})$$

654 where the sum is taken over all  $B$  barcodes.

655 If the total number of reads is given by Equation S25, the array with the number of reads for  
656 each barcode at time  $t$ ,  $\underline{r}_t$  is then distributed as

$$\underline{r}_t \sim \text{Multinomial}(n_t, \underline{f}_t), \quad (\text{S26})$$

657 where each of the  $B$  entries of the frequency vector  $\underline{f}_t$  is a function of the  $\underline{\lambda}_t$  vector, given  
658 by

$$f_t^{(b)} \equiv f_t^{(b)}(\underline{\lambda}_t) = \frac{\lambda_t^{(b)}}{\sum_{b'=1}^B \lambda_t^{(b')}}. \quad (\text{S27})$$

659 In other words, we can think of the  $B$  barcode counts as independent Poisson samples or as a  
660 single multinomial draw with a random number of total draws,  $n_t$ , and the frequency vector  
661  $\underline{f}_t$  we are interested in. Notice that Equation S27 is a deterministic function that connects  
662 the Poisson parameters to the frequencies. Therefore, we have the equivalence that

$$\pi(\underline{f}_t | \underline{r}_t) = \pi(\underline{\lambda}_t | \underline{r}_t), \quad (\text{S28})$$

663 meaning that the uncertainty comes from the  $\underline{\lambda}_t$  vector. By Bayes theorem, we therefore  
664 write

$$\pi(\underline{\lambda}_t | n_t, \underline{r}_t) \propto \pi(n_t, \underline{r}_t | \underline{\lambda}_t) \pi(\underline{\lambda}_t), \quad (\text{S29})$$

665 where we explicitly include the dependence on  $n_t$ . This does not affect the distribution or  
666 brings more uncertainty because  $\underline{r}_t$  already contains all the information to compute  $n_t$  since

$$n_t = \sum_{b=1}^B r_t^{(b)}. \quad (\text{S30})$$

667 But adding the variable allows us to factorize Equation S29 as

$$\pi(\underline{\lambda}_t | n_t, \underline{r}_t) \propto \pi(\underline{r}_t | n_t, \underline{\lambda}_t) \pi(n_t | \underline{\lambda}_t) \pi(\underline{\lambda}_t) \quad (\text{S31})$$

668 We then have

$$\underline{r}_t | n_t, \underline{\lambda}_t \sim \text{Multinomial}(n_t, \underline{f}_t(\underline{\lambda}_t)). \quad (\text{S32})$$

669 Furthermore, we have

$$n_t | \underline{\lambda}_t \sim \text{Poiss} \left( \sum_{b=1}^B \lambda_t^{(b)} \right).$$

670 {#eq=freq\_n\_bayes} Finally, for our prior  $\pi(\underline{\lambda}_t)$ , we first assume each parameter is indepen-  
671 dent, i.e.,

$$\pi(\underline{\lambda}_t) = \prod_{b=1}^B \pi(\lambda_t^{(b)}).$$

672 A reasonable prior for each  $\lambda_t^{(b)}$  representing the expected number of reads for barcode  $b$   
673 should span several orders of magnitude. Furthermore, we assume that no barcode in the  
674 dataset ever goes extinct. Thus, no frequency can equal zero, facilitating the computation  
675 of the log frequency ratios needed to infer the relative fitness. The log-normal distribution  
676 satisfies these constraints; therefore, for the prior, we assume

$$\lambda_t^{(b)} \sim \log \mathcal{N}(\mu_{\lambda_t^{(b)}}, \sigma_{\lambda_t^{(b)}}), \quad (\text{S33})$$

677 with  $\mu_{\lambda_t^{(b)}}, \sigma_{\lambda_t^{(b)}}$  as the user-defined parameters that characterize the prior distribution.

## 678 Summary

679 Putting all the pieces developed in this section together gives a term for our inference of the  
680 form

$$\pi(\underline{F} | \underline{R}) \propto \prod_{t=1}^T \left\{ \pi(r_t | n_t, \underline{\lambda}_t) \pi(n_t | \underline{\lambda}_t) \left[ \prod_{b=1}^B \pi(\lambda_t^{(b)}) \right] \right\} \quad (\text{S34})$$

681 where

$$r_t | n_t, \underline{\lambda}_t \sim \text{Multinomial}(n_t, f_t(\underline{\lambda}_t)), \quad (\text{S35})$$

$$n_t | \underline{\lambda}_t \sim \text{Poiss} \left( \sum_{b=1}^B \lambda_t^{(b)} \right). \quad (\text{S36})$$

683 and

$$\lambda_t^{(b)} \sim \log \mathcal{N}(\mu_{\lambda_t^{(b)}}, \sigma_{\lambda_t^{(b)}}), \quad (\text{S37})$$

## 684 Population mean fitness uncertainty $\pi(\bar{s}_T | \underline{F}, \underline{R})$

685 Next, we turn our attention to the problem of determining the population mean fitnesses  $\bar{s}_T$ .  
686 First, we notice that our fitness model in Equation 3 does not include the value of the raw  
687 reads. They enter the calculation indirectly through the inference of the frequency values we  
688 developed in Section . This means that we can remove the conditioning of the value of  $\bar{s}_T$   
689 on the number of reads, obtaining a simpler probability function

$$\pi(\bar{s}_T | \underline{F}, \underline{R}) = \pi(\bar{s}_T | \underline{F}). \quad (\text{S38})$$

690 Moreover, our fitness model does not directly explain how the population mean fitness evolves  
691 over time. In other words, our model cannot explicitly compute the population mean fitness  
692 at time  $t + 1$  from the information we have about time  $t$ . Given this model limitation, we are

693 led to assume that we must infer each  $\bar{s}_t$  independently. Expressing this for our inference  
 694 results in

$$\pi(\underline{\bar{s}}_T \mid \underline{\underline{F}}) = \prod_{t=1}^{T-1} \pi(\bar{s}_t \mid \underline{f}_t, \underline{f}_{t+1}), \quad (\text{S39})$$

695 where we split our matrix  $\underline{\underline{F}}$  for each time point and only kept the conditioning on the relevant  
 696 frequencies needed to compute the mean fitness at time  $t$ .

697 Although our fitness model in Equation 3 also includes the relative fitness  $s^{(m)}$ , to infer the  
 698 population mean fitness we only utilize data from the neutral lineages that, by definition,  
 699 have a relative fitness  $s^{(n)} = 0$ . Therefore, the conditioning on Equation S39 can be further  
 700 simplified by only keeping the frequencies of the neutral lineages, i.e.,

$$\pi(\bar{s}_t \mid \underline{f}_t, \underline{f}_{t+1}) = \pi(\bar{s}_t \mid \underline{f}_t^N, \underline{f}_{t+1}^N). \quad (\text{S40})$$

701 Recall that in Section we emphasized that the frequencies  $f_t^{(n)}$  do not represent the true  
 702 frequency of a particular lineage in the population but rather a “normalized number of  
 703 cells.” Therefore, it is safe to assume each of the  $N$  neutral lineages’ frequencies is changing  
 704 independently. The correlation of how increasing the frequency of one lineage will decrease  
 705 the frequency of others is already captured in the model presented in Section . Thus, we  
 706 write

$$\pi(\bar{s}_t \mid \underline{f}_t^N, \underline{f}_{t+1}^N) = \prod_{n=1}^N \pi(\bar{s}_t \mid f_t^{(n)}, f_{t+1}^{(n)}). \quad (\text{S41})$$

707 Now, we can focus on one of the terms on the right-hand side of Equation S41. Writing  
 708 Bayes theorem results in

$$\pi(\bar{s}_t \mid f_t^{(n)}, f_{t+1}^{(n)}) \propto \pi(f_t^{(n)}, f_{t+1}^{(n)} \mid \bar{s}_t) \pi(\bar{s}_t). \quad (\text{S42})$$

709 Notice the likelihood defines the joint distribution of neutral barcode frequencies conditioned  
 710 on the population mean fitness. However, rewriting our fitness model in Equation 3 for a  
 711 neutral lineage to leave frequencies on one side and fitness on the other results in

$$\frac{f_{t+1}^{(n)}}{f_t^{(n)}} = e^{-\bar{s}_t \tau}. \quad (\text{S43})$$

712 Equation S43 implies that our fitness model only relates **the ratio** of frequencies and not the  
 713 individual values. To get around this complication, we define

$$\gamma_t^{(b)} \equiv \frac{f_{t+1}^{(b)}}{f_t^{(b)}}, \quad (\text{S44})$$

714 as the ratio of frequencies between two adjacent time points for any barcode  $b$ . This allows  
 715 us to rewrite the joint distribution  $\pi(f_t^{(n)}, f_{t+1}^{(n)} \mid \bar{s}_t)$  as

$$\pi(f_t^{(n)}, f_{t+1}^{(n)} \mid \bar{s}_t) = \pi(f_t^{(n)}, \gamma_t^{(n)} \mid \bar{s}_t). \quad (\text{S45})$$

716 Let us rephrase this subtle but necessary change of variables since it is a key part of the  
 717 inference problem: our series of independence assumptions lead us to Equation S42 that  
 718 relates the value of the population mean fitness  $\bar{s}_t$  to the frequency of a neutral barcode at  
 719 times  $t$  and  $t + 1$ . However, as shown in Equation S43, our model functionally relates the  
 720 ratio of frequencies—that we defined as  $\gamma_t^{(n)}$ —and not the independent frequencies to the  
 721 mean fitness. Therefore, instead of writing for the likelihood the joint distribution of the  
 722 frequency values at times  $t$  and  $t + 1$  conditioned on the mean fitness, we write the joint  
 723 distribution of the barcode frequency at time  $t$  and the ratio of the frequencies. These **must**  
 724 **be** equivalent joint distributions since there is a one-to-one mapping between  $\gamma_t^{(n)}$  and  $f_{t+1}^{(n)}$   
 725 for a given value of  $f_t^{(n)}$ . Another way to phrase this is to say that knowing the frequency at  
 726 time  $t$  and at time  $t + 1$  provides the same amount of information as knowing the frequency  
 727 at time  $t$  and the ratio of the frequencies. This is because if we want to obtain  $f_{t+1}^{(n)}$  given  
 728 this information, we simply compute

$$f_{t+1}^{(n)} = \gamma_t^{(n)} f_t^{(n)}. \quad (\text{S46})$$

729 The real advantage of rewriting the joint distribution as in Equation S45 comes from splitting  
 730 this joint distribution as a product of conditional distributions of the form

$$\pi(f_t^{(n)}, \gamma_t^{(n)} | \bar{s}_t) = \pi(f_t^{(n)} | \gamma_t^{(n)}, \bar{s}_t) \pi(\gamma_t^{(n)} | \bar{s}_t). \quad (\text{S47})$$

731 Written in this form, we can finally propose a probabilistic model for how the mean fitness  
 732 relates to the frequency ratios we determine in our experiments. The second term on the  
 733 right-hand side of Equation S47 relates how the determined frequency ratio  $\gamma_t^{(b)}$  relates to  
 734 the mean fitness  $\bar{s}_t$ . From Equation S43 and Equation S44, we can write

$$\ln \gamma_t^{(n)} = -\bar{s}_t + \varepsilon_t^{(n)}, \quad (\text{S48})$$

735 where, for simplicity, we set  $\tau = 1$ . Note that we added an extra term,  $\varepsilon_t^{(n)}$ , characterizing  
 736 the deviations of the measurements from the theoretical model. We assume these errors are  
 737 normally distributed with mean zero and some standard deviation  $\sigma_t$ , implying that

$$\ln \gamma_t^{(n)} | \bar{s}_t, \sigma_t \sim \mathcal{N}(-\bar{s}_t, \sigma_t), \quad (\text{S49})$$

738 where we include the nuisance parameter  $\sigma_t$  to be determined. If we assume the log frequency  
 739 ratio is normally distributed, this implies the frequency ratio itself is distributed log-normal.  
 740 This means that

$$\gamma_t^{(n)} | \bar{s}_t, \sigma_t \sim \log \mathcal{N}(-\bar{s}_t, \sigma_t). \quad (\text{S50})$$

741 Having added the nuisance parameter  $\sigma_t$  implies that we must update Equation S42 to

$$\pi(\bar{s}_t, \sigma_t | f_t^{(n)}, f_{t+1}^{(n)}) \propto \pi(f_t^{(n)}, \gamma_t^{(n)} | \bar{s}_t, \sigma_t) \pi(\bar{s}_t) \pi(\sigma_t), \quad (\text{S51})$$

742 where we assume the prior for each parameter is independent, i.e.,

$$\pi(\bar{s}_t, \sigma_t) = \pi(\bar{s}_t) \pi(\sigma_t). \quad (\text{S52})$$

743 For numerical stability, we will select weakly-informative priors for both of these parameters.  
 744 In the case of the nuisance parameter  $\sigma_t$ , the prior must be restricted to positive values only,  
 745 since standard deviations cannot be negative.

746 For the first term on the right-hand side of Equation S47,  $\pi(f_t^{(n)} | \gamma_t^{(n)}, \bar{s}_t)$ , we remove the  
 747 conditioning on the population mean fitness since it does not add any information on top of  
 748 what the frequency ratio  $\gamma_t^{(n)}$  already gives. Therefore, we have

$$\pi(f_t^{(n)} | \gamma_t^{(n)}, \bar{s}_t) = \pi(f_t^{(n)} | \gamma_t^{(n)}). \quad (\text{S53})$$

749 The right-hand side of Equation S53 asks us to compute the probability of observing a  
 750 frequency value  $f_t^{(n)}$  given that we get to observe the ratio  $\gamma_t^{(n)}$ . If the ratio happened to be  
 751  $\gamma_t^{(n)} = 2$ , we could have  $f_{t+1}^{(n)} = 1$  and  $f_{t+1}^{(n)} = 0.5$ , for example. Although, it would be equally  
 752 likely that  $f_{t+1}^{(n)} = 0.6$  and  $f_{t+1}^{(n)} = 0.3$  or  $f_{t+1}^{(n)} = 0.1$  and  $f_{t+1}^{(n)} = 0.05$  for that matter. If we  
 753 only get to observe the frequency ratio  $\gamma_t^{(n)}$ , we know that the numerator  $f_{t+1}^{(n)}$  can only take  
 754 values between zero and one, all of them being equally likely given only the information on  
 755 the ratio. As a consequence, the value of the frequency in the denominator  $f_t^{(n)}$  is restricted  
 756 to fall in the range

$$f_t^{(n)} \in \left(0, \frac{1}{\gamma_t^{(n)}}\right]. \quad (\text{S54})$$

757 A priori, we do not have any reason to favor any value over any other, therefore it is natural  
 758 to write

$$f_t^{(n)} | \gamma_t^{(n)} \sim \text{Uniform}\left(0, \frac{1}{\gamma_t^{(n)}}\right). \quad (\text{S55})$$

## 759 Summary

760 Putting all the pieces we have developed in this section together results in an inference for  
 761 the population mean fitness values of the form

$$\pi(\bar{s}_T, \underline{\sigma}_T | \underline{F}) \propto \prod_{t=1}^{T-1} \left\{ \prod_{n=1}^N [\pi(f_t^{(n)} | \gamma_t^{(n)}) \pi(\gamma_t^{(n)} | \bar{s}_t, \sigma_t)] \pi(\bar{s}_t) \pi(\sigma_t) \right\}, \quad (\text{S56})$$

762 where we have

$$f_t^{(n)} | \gamma_t^{(n)} \sim \text{Uniform}\left(0, \frac{1}{\gamma_t^{(n)}}\right), \quad (\text{S57})$$

$$\gamma_t^{(n)} | \bar{s}_t, \sigma_t \sim \log \mathcal{N}(\bar{s}_t, \sigma_t), \quad (\text{S58})$$

$$\bar{s}_t \sim \mathcal{N}(0, \sigma_{\bar{s}_t}), \quad (\text{S59})$$

765 and

$$\sigma_t \sim \log \mathcal{N}(\mu_{\sigma_t}, \sigma_{\sigma_t}), \quad (\text{S60})$$

766 where  $\sigma_{\bar{s}_t}$ ,  $\mu_{\sigma_t}$ , and  $\sigma_{\sigma_t}$  are user-defined parameters.

767 **Mutant relative fitness uncertainty**  $\pi(\underline{s}^M \mid \bar{s}_T, \underline{F}, \underline{R})$

768 The last piece of our inference is the piece that we care about the most: the probability  
 769 distribution of all the mutants' relative fitness, given the inferred population mean fitness  
 770 and the frequencies. First, we assume that all fitness values are independent of each other.  
 771 This allows us to write

$$\pi(\underline{s}^M \mid \bar{s}_T, \underline{F}, \underline{R}) = \prod_{m=1}^M \pi(s^{(m)} \mid \bar{s}_T, \underline{F}, \underline{R}). \quad (\text{S61})$$

772 Furthermore, as was the case with the population mean fitness, our fitness model relates  
 773 frequencies, not raw reads. Moreover, the fitness value of mutant  $m$  only depends on the  
 774 frequencies of such mutant. Therefore, we can simplify the conditioning to

$$\pi(s^{(m)} \mid \bar{s}_T, \underline{F}, \underline{R}) = \pi(s^{(m)} \mid \bar{s}_T, \underline{f}^{(m)}), \quad (\text{S62})$$

775 where

$$\underline{f}^{(m)} = (f_0^{(m)}, f_1^{(m)}, \dots, f_T^{(m)})^\dagger, \quad (\text{S63})$$

776 is the vector containing the frequency time series for mutant  $m$ . Writing Bayes' theorem for  
 777 the right-hand side of Equation S62 results in

$$\pi(s^{(m)} \mid \bar{s}_T, \underline{f}^{(m)}) \propto \pi(\underline{f}^{(m)} \mid \bar{s}_T, s^{(m)}) \pi(s^{(m)} \mid \bar{s}_T). \quad (\text{S64})$$

778 Notice the conditioning on the mean fitness values  $\bar{s}_T$  is not inverted since we already inferred  
 779 these values.

780 Following the logic used in Section , let us define

$$\underline{\gamma}^{(m)} = (\gamma_0^{(m)}, \gamma_1^{(m)}, \dots, \gamma_{T-1}^{(m)})^\dagger, \quad (\text{S65})$$

781 where each entry  $\gamma_t^{(m)}$  is defined by Equation S44. In the same way we rewrote the joint  
 782 distribution between two adjacent time point frequencies to the joint distribution between  
 783 one of the frequencies and the ratio of both frequencies in Equation S45, we can rewrite the  
 784 joint distribution of the frequency time series for mutant  $m$  as

$$\pi(\underline{f}^{(m)} \mid \bar{s}_T, s^{(m)}) = \pi(f_0^{(m)}, \underline{\gamma}^{(m)} \mid \bar{s}_T, s^{(m)}). \quad (\text{S66})$$

785 One can think about Equation S66 as saying that knowing the individual frequencies at each  
 786 time point contain equivalent information as knowing the initial frequency and the subsequent  
 787 ratios of frequencies. This is because if we want to know the value of  $f_1^{(m)}$  given the ratios,  
 788 we only need to compute

$$f_1^{(m)} = \gamma_0^{(m)} f_0^{(m)}. \quad (\text{S67})$$

789 Moreover, if we want to know  $f_2^{(m)}$ , we have

$$f_2^{(m)} = \gamma_1^{(m)} f_1^{(m)} = \gamma_1^{(m)} (\gamma_0^{(m)} f_0^{(m)}), \quad (\text{S68})$$

790 and so on. We can then write the joint distribution on the right-hand side of Equation S66  
 791 as a product of conditional distributions of the form

$$\begin{aligned} \pi(f_0^{(m)}, \underline{\gamma}^{(m)} | \bar{s}_T, s^{(m)}) &= \pi(f_0^{(m)} | \gamma_0^{(m)}, \dots, \gamma_{T-1}^{(m)}, \bar{s}_T, s^{(m)}) \times \\ &\quad \pi(\gamma_0^{(m)} | \gamma_1^{(m)}, \dots, \gamma_{T-1}^{(m)}, \bar{s}_T, s^{(m)}) \times \\ &\quad \pi(\gamma_1^{(m)} | \gamma_2^{(m)}, \dots, \gamma_{T-1}^{(m)}, \bar{s}_T, s^{(m)}) \times \\ &\quad \vdots \\ &\quad \pi(\gamma_{T-2}^{(m)} | \gamma_{T-1}^{(m)}, \bar{s}_T, s^{(m)}) \times \\ &\quad \pi(\gamma_{T-1}^{(m)} | \bar{s}_T, s^{(m)}). \end{aligned} \tag{S69}$$

792 Writing the fitness model in Equation 3 as

$$\gamma_t^{(m)} = \frac{f_{t+1}^{(m)}}{f_t^{(m)}} = e^{(s^{(m)} - s_t)\tau},$$

793 reveals that the value of each of the ratios  $\gamma_t^{(m)}$  only depends on the corresponding fitness  
 794 value  $\bar{s}_t$  and the relative fitness  $s^{(m)}$ . Therefore, we can remove most of the conditioning  
 795 on the right-hand side of Equation S69, resulting in a much simpler joint distribution of the  
 796 form

$$\begin{aligned} \pi(f_0^{(m)}, \underline{\gamma}^{(m)} | \bar{s}_T, s^{(m)}) &= \pi(f_0^{(m)} | \gamma_0^{(m)}) \times \\ &\quad \pi(\gamma_0^{(m)} | \bar{s}_0, s^{(m)}) \times \\ &\quad \pi(\gamma_1^{(m)} | \bar{s}_1, s^{(m)}) \times \\ &\quad \vdots \\ &\quad \pi(\gamma_{T-2}^{(m)} | \bar{s}_{T-2}, s^{(m)}) \times \\ &\quad \pi(\gamma_{T-1}^{(m)} | \bar{s}_{T-1}, s^{(m)}), \end{aligned} \tag{S70}$$

797 where for the first term on the right-hand side of Equation S70 we apply the same logic as in  
 798 Equation S53 to remove all other dependencies. We emphasize that although Equation S70  
 799 looks like a series of independent inferences, the value of the relative fitness  $s^{(m)}$  is shared  
 800 among all of them. This means that the parameter is not inferred individually for each time  
 801 point, resulting in different estimates of the parameter, but each time point contributes  
 802 independently to the inference of a single estimate of  $s^{(m)}$ .

803 Using equivalent arguments to those in Section , we assume

$$f_0^{(m)} | \gamma_0^{(m)} \sim \text{Uniform}\left(0, \frac{1}{\gamma_0^{(m)}}\right),$$

804 and

$$\gamma_t^{(m)} | \bar{s}_t, s^{(m)}, \sigma^{(m)} \sim \log \mathcal{N}(s^{(m)} - \bar{s}_t, \sigma^{(m)}), \tag{S71}$$

805 where we add the nuisance parameter  $\sigma^{(m)}$  to the inference. Notice that this parameter is not  
 806 indexed by time. This means that we assume the deviations from the theoretical prediction  
 807 do not depend on time, but only on the mutant. Adding the nuisance parameter demands us  
 808 to update Equation S64 to

$$\pi(s^{(m)}, \sigma^{(m)} | \bar{s}_T, \underline{f}^{(m)}) \propto \pi(\underline{f}^{(m)} | \bar{s}_T, s^{(m)}, \sigma^{(m)}) \pi(s^{(m)}) \pi(\sigma^{(m)}), \quad (\text{S72})$$

809 where we assume independent priors for both parameters. We also removed the conditioning  
 810 on the values of the mean fitness as knowing such values does not change our prior information  
 811 about the possible range of values that the parameters can take. As with the priors on  
 812 Section , we will assign weakly-informative priors to these parameters.

813 **Summary**

814 With all pieces in place, we write the full inference of the relative fitness values as

$$\pi(\underline{s}^M, \underline{\sigma}^M | \bar{s}_T, \underline{F}) \propto \prod_{m=1}^M \left\{ \pi(f_0^{(m)} | \gamma_0^{(m)}) \prod_{t=0}^{T-1} [\pi(\gamma_t^{(m)} | \bar{s}_t, s^{(m)}, \sigma^{(m)})] \pi(s^{(m)}) \pi(\sigma^{(m)}) \right\}, \quad (\text{S73})$$

815 where

$$f_0^{(m)} | \gamma_0^{(m)} \sim \text{Uniform}\left(0, \frac{1}{\gamma_0^{(m)}}\right), \quad (\text{S74})$$

$$\gamma_t^{(m)} | \bar{s}_t, s^{(m)}, \sigma^{(m)} \sim \log \mathcal{N}(s^{(m)} - \bar{s}_t, \sigma^{(m)}), \quad (\text{S75})$$

$$s^{(m)} \sim \mathcal{N}(0, \sigma_{s^{(m)}}), \quad (\text{S76})$$

816 and

$$\sigma^{(m)} \sim \log \mathcal{N}(\mu_{\sigma^{(m)}}, \sigma_{\sigma^{(m)}}), \quad (\text{S77})$$

817 where  $\sigma_{s^{(m)}}, \mu_{\sigma^{(m)}},$  and  $\sigma_{\sigma^{(m)}}$  are user-defined parameters.

818 **Hierarchical models for multiple experimental replicates**

819 As detailed in Section of the main text, we define a Bayesian hierarchical model to analyze data  
 820 from multiple experimental replicates. The implementation requires only slightly modifying  
 821 the base model detailed in the previous sections. The hierarchical model defines a hyper-  
 822 fitness parameter  $\theta^{(m)}$  for every non-neutral barcode. We can thus collect all of the  $M$   
 823 hyperparameters in an array of the form

$$\underline{\theta}^M = (\theta^{(1)}, \dots, \theta^{(M)})^\dagger. \quad (\text{S78})$$

824 Our data now consists of a series of matrices  $\underline{\underline{R}}_{[j]}$ , where the subindex  $[j]$  refers to the  $j$ -th  
 825 experimental replicate. These matrices need not have the same number of rows, as the time

828 points measured for each replicate can vary. The statistical model we must define is then of  
 829 the form

$$\begin{aligned} \pi(\underline{\theta}^M, \{\underline{s}_{[j]}^M\}, \{\bar{s}_{T[j]}\}, \{\underline{F}_{[j]}\} \mid \{\underline{R}_{[j]}\}) &\propto \pi(\{\underline{R}_{[j]}\} \mid \underline{\theta}^M, \{\underline{s}_{[j]}^M\}, \{\bar{s}_{T[j]}\}, \{\underline{F}_{[j]}\}) \times \\ &\quad \pi(\underline{\theta}^M, \{\underline{s}_{[j]}^M\}, \{\bar{s}_{T[j]}\}, \{\underline{F}_{[j]}\}) \end{aligned} \quad (\text{S79})$$

830 where the parameters within curly braces with subindex  $[j]$  indicate one set of parameters per  
 831 experimental replicate. For example,

$$\{\underline{s}_{[j]}^M\} = \{\underline{s}_{[1]}^M, \underline{s}_{[2]}^M, \dots, \underline{s}_{[E]}^M\}, \quad (\text{S80})$$

832 where  $E$  is the number of experimental replicates.

833 Given the dependencies between the variables, we can factorize Equation S79 to be of the  
 834 form

$$\begin{aligned} \pi(\underline{\theta}^M, \{\underline{s}_{[j]}^M\}, \{\bar{s}_{T[j]}\}, \{\underline{F}_{[j]}\} \mid \{\underline{R}_{[j]}\}) &= \pi(\underline{\theta}^M, \{\underline{s}_{[j]}^M\} \mid \{\bar{s}_{T[j]}\}, \{\underline{F}_{[j]}\}) \times \\ &\quad \pi(\{\bar{s}_{T[j]}\} \mid \{\underline{F}_{[j]}\}) \times \\ &\quad \pi(\{\underline{F}_{[j]}\} \mid \{\underline{R}_{[j]}\}) \end{aligned} \quad (\text{S81})$$

835 Furthermore, the hierarchical structure only connects the replicates via the relative fitness  
 836 parameters. This means that the population mean fitness values and the frequencies can  
 837 be independently inferred for each dataset. This allows us to rewrite the right-hand side of  
 838 Equation S81 as

$$\begin{aligned} \pi(\underline{\theta}^M, \{\underline{s}_{[j]}^M\}, \{\bar{s}_{T[j]}\}, \{\underline{F}_{[j]}\} \mid \{\underline{R}_{[j]}\}) &= \pi(\underline{\theta}^M, \{\underline{s}_{[j]}^M\} \mid \{\bar{s}_{T[j]}\}, \{\underline{F}_{[j]}\}) \times \\ &\quad \prod_{j=1}^E \left[ \pi(\bar{s}_{T[j]} \mid \underline{F}_{[j]}) \pi(\underline{F}_{[j]} \mid \underline{R}_{[j]}) \right]. \end{aligned} \quad (\text{S82})$$

839 The terms inside the square brackets in Equation S82 take the same functional form as those  
 840 derived in Section and Section . Therefore, to implement the desired hierarchical model, we  
 841 only need to focus on the first term on the right-hand side of Equation S82. A way to think  
 842 about the structure of the hierarchical model is as follows: imagine each genotype as a “*true*”  
 843 relative fitness value. However, every time we perform an experiment, small variations in the  
 844 biotic and abiotic conditions—also known as batch effects—might result in small deviations  
 845 from this value. We model this by defining a distribution for the hyper-fitness parameter—the  
 846 ground truth we are interested in—and having each experimental replicate sample from  
 847 this hyper-parameter distribution to determine the “*local*” fitness value. The wider the  
 848 hyper-parameter distribution is the more variability between experimental replicates.

849 Writing Bayes’ theorem for the first term in Equation S82 results in

$$\pi(\underline{\theta}^M, \{\underline{s}_{[j]}^M\} \mid \{\underline{F}_{[j]}\}, \{\bar{s}_{T[j]}\}) \propto \pi(\{\underline{F}_{[j]}\} \mid \underline{\theta}^M, \{\underline{s}_{[j]}^M\}, \{\bar{s}_{T[j]}\}) \pi(\underline{\theta}^M, \{\underline{s}_{[j]}^M\} \mid \{\bar{s}_{T[j]}\}), \quad (\text{S83})$$

850 where we leave the conditioning on the population mean fitness as we did in Section . This  
 851 expression can be simplified in two ways. First, the frequency values for each experimental  
 852 replicate depend directly on the local fitness values and the corresponding population mean  
 853 fitness, as the relationship between experimental replicates only occurs through the relative  
 854 fitness values. Therefore, we can write

$$\pi(\underline{\theta}^M, \{s_{[j]}^M\} \mid \{\underline{F}_{[j]}\}, \{\bar{s}_{T[j]}\}) \propto \prod_{j=1}^E \left[ \pi(\underline{F}_{[j]} \mid s_{[j]}^M, \bar{s}_{T[j]}) \right] \pi(\underline{\theta}^M, \{s_{[j]}^M\} \mid \{\bar{s}_{T[j]}\}). \quad (\text{S84})$$

855 Second, the relationship between the hyper-fitness and the local fitness values allows us to  
 856 write their joint distribution as a conditional distribution where local fitness values depend on  
 857 the global hyper-fitness value, obtaining

$$\pi(\underline{\theta}^M, \{s_{[j]}^M\} \mid \{\underline{F}_{[j]}\}, \{\bar{s}_{T[j]}\}) \propto \prod_{j=1}^E \left[ \pi(F_{[j]} \mid s_{[j]}^M, \bar{s}_{T[j]}) \pi(s_{[j]}^M \mid \underline{\theta}^M) \right] \pi(\underline{\theta}^M). \quad (\text{S85})$$

858 Notice we removed the conditioning on the population mean fitness as our prior expectations  
 859 of what the global hyper-fitness or local fitness value might be do not depend on these  
 860 nuisance parameters.

861 The first term on the right-hand side of Equation S85 takes the same functional form as the  
 862 one derived in Section . Therefore, all we are left with is to determine the functional forms  
 863 for the hyper-prior  $\pi(\underline{\theta}^M)$ , and the conditional probability  $\pi(s_{[j]}^M \mid \underline{\theta}^M)$ . In analogy to the  
 864 assumptions used for the fitness values in Section , we define the value of each hyper-fitness  
 865 as independent. This means that we have

$$\pi(\underline{\theta}^M) = \prod_{m=1}^M \pi(\theta^{(m)}). \quad (\text{S86})$$

866 Furthermore, we assume this prior is of the form

$$\theta^{(m)} \sim \mathcal{N}(\mu_{\theta^{(m)}}, \sigma_{\theta^{(m)}}), \quad (\text{S87})$$

867 where  $\mu_{\theta^{(m)}}$  and  $\sigma_{\theta^{(m)}}$  are user-defined parameters encoding the prior expectations on the  
 868 fitness values.

869 For the conditional distribution  $\pi(s_{[j]}^M \mid \underline{\theta}^M)$ , we use the so-called non-centered parametrization  
 870 that avoids some of the intrinsic degeneracies associated with hierarchical models<sup>13</sup>. We  
 871 invite the reader to check [this excellent blog](#) explaining the difficulties of working with  
 872 hierarchical models. This non-centered parameterization implies that we introduce two  
 873 nuisance parameters such that the local fitness  $s_{[j]}^{(m)}$  is computed as

$$s_{[j]}^{(m)} = \theta^{(m)} + (\tau_{[j]}^{(m)} \times \xi_{[j]}^{(m)}), \quad (\text{S88})$$

874 where  $\theta^{(m)}$  is the corresponding genotype hyper-fitness value,  $\xi_{[j]}^{(m)}$  is a standard normal  
 875 random variable, i.e.,

$$\xi_{[j]}^{(m)} \sim \mathcal{N}(0, 1), \quad (\text{S89})$$

876 that allows deviations from the hyper-fitness value to be either positive or negative, and  $\tau_{[j]}^{(m)}$   
877 is a strictly positive random variable that characterizes the deviation of the local fitness value  
878 from the global hyper-fitness. We assume

$$\tau_{[j]}^{(m)} \sim \log \mathcal{N}(\mu_{\tau_{[j]}^{(m)}}, \sigma_{\tau_{[j]}^{(m)}}) \quad (\text{S90})$$

879 where  $\mu_{\tau_{[j]}^{(m)}}$  and  $\sigma_{\tau_{[j]}^{(m)}}$  are user-defined parameters capturing the expected magnitude of the  
880 batch effects.

### 881 Defining prior probabilities

882 One aspect commonly associated—in both positive and negative ways—to Bayesian analysis  
883 is the definition of prior probabilities. On the one hand, the naive textbook version of Bayesian  
884 analysis defines the prior as encoding the information we have about the inference in question  
885 before acquiring any data. This is the “ideal” use of priors that, whenever possible, should  
886 be implemented. On the other hand, for most practitioners of Bayesian statistics in the age  
887 of big data, the definition of prior becomes a tool to ensure the convergence of sampling  
888 algorithms such as MCMC<sup>25</sup>. However, for our particular problem, although we deal with  
889 large amounts of data (inferences can be made for  $> 10K$  barcodes over multiple time points,  
890 resulting in  $> 100K$  parameters), each barcode has very little data, as they are measured  
891 only once per time point over  $< 10$  growth-dilution cycles. Furthermore, it is incredibly  
892 challenging to understand the noise sources related to culturing conditions, DNA extraction,  
893 library preparation, etc., and encode them into reasonable prior distributions.

894 Empirically, our approach for this work defined the priors based solely on the neutral lineage  
895 data, as they represent the only repeated measurements of a single genotype in our experi-  
896 mental design. We acknowledge that defining the priors after observing the data might be  
897 considered an incoherent inference. However, as expressed by Gelman et al. [25]

898 Incoherence is an unavoidable aspect of much real-world data analysis; and,  
899 indeed, one might argue that as scientists we learn the most from the anomalies  
900 and reassessments associated with episodes of incoherence.

901 With this in mind, we leave it to the reader to judge the selection of priors. Furthermore,  
902 the software package associated with this work, BarBay.jl, is written so that users can  
903 experiment with different prior selection criteria that fit their needs. We strongly advocate  
904 that statistics should not be done in a black-box fit-all tool mindset but rather as a formal  
905 way to encode the assumptions behind the analysis, subject to constructive criticism. With  
906 this philosophical baggage behind us, let us now focus on how the priors used for this work  
907 were selected.

908 **Naive neutral lineage-based priors**

909 For the base model presented in this work, the user-defined prior parameters include the  
 910 following:

- 911     ■ Prior on population mean fitness (one per pair of adjacent time points)

$$\bar{s}_t \sim \mathcal{N}(\mu_{\bar{s}_t}, \sigma_{\bar{s}_t}). \quad (\text{S91})$$

- 912     ■ Prior on standard deviation associated with neutral lineages likelihood function (one  
 913       per pair of adjacent time points)

$$\sigma_t \sim \log \mathcal{N}(\mu_{\sigma_t}, \sigma_{\sigma_t}). \quad (\text{S92})$$

- 914     ■ Prior on relative fitness (one per non-neutral barcode)

$$s^{(m)} \sim \mathcal{N}(\mu_{s^{(m)}}, \sigma_{s^{(m)}}). \quad (\text{S93})$$

- 915     ■ Prior on standard deviation associated with non-neutral lineages likelihood function  
 916       (one per non-neutral barcode)

$$\sigma^{(m)} \sim \log \mathcal{N}(\mu_{\sigma^{(m)}}, \sigma_{\sigma^{(m)}}) \quad (\text{S94})$$

917 The BarBay.jl package includes a function `naive_prior` within the `stats` module. This  
 918 function utilizes the data from the neutral lineages to determine some of the prior parameters  
 919 to facilitate the inference algorithm's numerical convergence. In particular, it defines the  
 920 population mean fitness parameter  $\mu_{\bar{s}_t}$  as

$$\mu_{\bar{s}_t} = \frac{1}{N} \sum_{n=1}^N -\ln \left( \frac{r_{t+1}^{(n)}}{r_t^{(n)}} \right), \quad (\text{S95})$$

921 where  $N$  is the number of neutral lineages and  $r_t^{(n)}$  is the number of neutral lineages. In  
 922 other words, it defines the mean of the prior distribution as the mean of what one naively  
 923 would compute from the neutral lineages, discarding cases where the ratio diverges because  
 924 the denominator  $r_t^{(n)} = 0$ . For the variance parameter, we chose a value  $\sigma_{\bar{s}_t} = 0.05$ .

925 Furthermore, the `naive_prior` function defines the mean of the variance parameter as the  
 926 standard deviation of the log frequency ratios for the neutral lineages, i.e.,

$$\mu_{\sigma_t} = \sqrt{\text{Var} \left( \frac{r_{t+1}^{(n)}}{r_t^{(n)}} \right)}, \quad (\text{S96})$$

927 where `Var` is the sample variance. This same value was utilized for the mean of the  
 928 non-neutral barcode variance  $\mu_{\sigma^{(m)}}$ . While we assign the corresponding variances to be  
 929  $\sigma_{\sigma_t} = \sigma_{\sigma^{(m)}} = 1$ .

930 **Posterior predictive checks**

931 Throughout the main text, we allude to the concept of posterior predictive checks as a formal  
 932 way to assess the accuracy of our inference pipeline. Here, we explain the mechanics behind  
 933 the computation of these credible regions, given the output of the inference.

934 Bayesian models encode what is known as a *generative model*. This statement means that in  
 935 our definition of the likelihood function and the prior distribution, we, as modelers, propose a  
 936 mathematical function that captures all relevant relationships between unobserved (latent)  
 937 variables. Therefore, when these latent variables are input into the mathematical model,  
 938 this function *generates* data that should be, in principle, indistinguishable from the real  
 939 observations if the model is a good account of the underlying processes involved in the  
 940 phenomena of interest. This generative model implies that once we run the inference process  
 941 and update our posterior beliefs about the state of the latent variables, we can input back the  
 942 inferred values to our model and generate synthetic data. Furthermore, we can repeat this  
 943 process multiple times to compute the range where we expect to observe our data conditioned  
 944 on the accuracy of the model.

945 For our specific scenario, recall that our objective is to infer the relative fitness of a non-neutral  
 946 lineage  $s^{(m)}$  along with nuisance parameters related to the population mean fitness at each  
 947 point,  $\bar{s}_t$ , and the barcode frequency time series  $\underline{f}^{(m)}$ . All these variables are related through  
 948 our fitness model (see Section in the main text)

$$f_{t+1}^{(m)} = f_t^{(m)} e^{(s^{(m)} - s_t)\tau}. \quad (\text{S97})$$

949 As we saw, it is convenient to rewrite Equation S97 as

$$\frac{1}{\tau} \ln \frac{f_{t+1}^{(m)}}{f_t^{(m)}} = (s^{(m)} - s_t). \quad (\text{S98})$$

950 Written in this way, we separate the quantities we can compute from the experimental  
 951 observations—the left-hand side of Equation S98 can be computed from the barcode reads—  
 952 from the latent variables.

953 Although we perform the joint inference over all barcodes in the present work, let us focus on  
 954 the inference task for a single barcode as if it were computed independently. For a non-neutral  
 955 barcode, our task consists of computing the posterior probability

$$\pi(\theta | \underline{r}^{(m)}) = \pi(s^{(m)}, \sigma^{(m)}, \underline{s}_t, \underline{f}^{(m)} | \underline{r}^{(m)}), \quad (\text{S99})$$

956 where  $\theta$  represents all parameters to be inferred and  $\underline{r}^{(m)}$  is the vector with the barcode raw  
 957 counts time series. The list of parameters are

- 958     ■  $s^{(m)}$ : The barcode's relative fitness.  
 959     ■  $\sigma^{(m)}$ : A nuisance parameter used in the likelihood to generate the data. This captures  
 960       the expected deviation from Equation S98

- 961     ▪  $\underline{s}_t$ : The vector with all population mean fitness for each pair of adjacent time points.  
 962     ▪  $\underline{f}^{(m)}$ : The vector with the barcode frequency time series.

963 Furthermore, let us define a naive estimate of the barcode frequency at time  $t$  as

$$\hat{f}_t^{(m)} = \frac{r_t^{(m)}}{\sum_{b=1}^B r_t^{(b)}}. \quad (\text{S100})$$

964 We can compute this quantity from the data by normalizing the raw barcode counts by  
 965 the sum of all barcode counts. Furthermore, we can compute a naive estimate of the log  
 966 frequency ratio from the raw barcode counts as

$$\ln \hat{\gamma}_t^{(m)} = \ln \frac{\hat{f}_{t+1}^{(m)}}{\hat{f}_t^{(m)}} \quad (\text{S101})$$

967 In our generative model, we assumed

$$\ln \gamma_t^{(m)} | \theta \sim \mathcal{N}(s^{(m)} - s_t, \sigma^{(m)}). \quad (\text{S102})$$

968 This implies that once we determine the posterior distribution of our parameters, we can  
 969 generate synthetic values of  $\ln \gamma_t^{(m)}$  that we can then compare with the values obtained from  
 970 applying Equation S101 and Equation S101 to the raw data.

971 In practice, to compute the posterior predictive checks, we generate multiple samples from  
 972 the posterior distribution  $\pi(\theta | \underline{r}^{(m)})$

$$\underline{\theta} = (\theta_1, \theta_2, \dots, \theta_N). \quad (\text{S103})$$

973 With these samples in hand, the BarBay.jl package includes the function `logfreq_ratio_bc_ppc`  
 974 for non-neutral barcodes that uses this set of posterior parameter samples to generate  
 975 samples from the distribution defined in Equation S102. For a large-enough number of  
 976 samples, we can then compute the desired percentiles—5, 68, and 95 percentiles in all figures  
 977 in the main text—that are equivalent to the corresponding credible regions. In other words,  
 978 the range of values of  $\ln \gamma_t^{(m)}$  generated by this bootstrap process can be used to compute  
 979 the region where we expect to find our raw estimates  $\ln \hat{\gamma}_t^{(m)}$  with the desired probability.  
 980 The package BarBay.jl includes an equivalent function, `logfreq_ratio_popmean_ppc`,  
 981 for neutral lineages.

## 982 Logistic growth simulation

983 In this section, we explain the simulations used to assess the validity of our inference pipeline.  
 984 Let us begin by assuming that, since the strains are grown for two full days in the experiment,  
 985 having left behind the exponential phase for almost an entire day, a simple exponential growth  
 986 of the form

$$\frac{dn_i}{dt} = \lambda_i n_i, \quad (\text{S104})$$

987 where  $n_i$  is the number of cells of strain  $i$ , and  $\lambda_i$  is the corresponding growth rate is not  
 988 enough. Instead, we will assume that the cells follow the logistic growth equation of the  
 989 form

$$\frac{dn_i}{dt} = \lambda_i n_i \left(1 - \frac{\sum_{j=1}^N n_j}{\kappa}\right), \quad (\text{S105})$$

990 where  $\kappa$  is the carrying capacity, and  $N$  is the total number of strains in the culture.

991 The inference method is based on the model that assumes that the time passed between  
 992 dilutions  $\tau \approx 8$  generations, the change in frequency for a mutant barcode can be approximated  
 993 from cycle  $t$  to the next cycle  $t + 1$  as

$$f_{t+1}^{(m)} = f_t^{(m)} e^{(s^{(m)} - \bar{s}_t)\tau}, \quad (\text{S106})$$

994 where  $s^{(m)}$  is the relative fitness for strain  $i$  compared to the ancestral strain and  $\bar{s}_t$  is  
 995 the mean fitness of the population at cycle  $t$ . To test this assumption, we implemented  
 996 a numerical experiment following the logistic growth model described in Equation S105.  
 997 Figure S2 shows an example of the deterministic trajectories for 50 labeled neutral lineages  
 998 and 1000 lineages of interest. The upper red curve that dominates the culture represents the  
 999 unlabeled ancestral strain included in the experimental design described in Section .

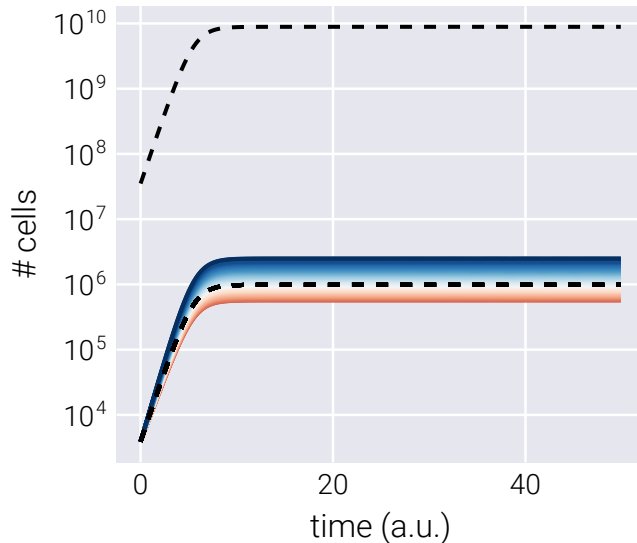


**Figure S2. Logistic growth simulation over single growth cycle.** The dashed line represents the neutral lineages, with the upper curve being the unlabeled neutral strain. Color curves represent the genotypes of interest colored by growth rate relative to the neutral lineage.

1000 To simulate multiple growth-dilution cycles, we take the population composition at the final  
 1001 time point and use it to initialize a new logistic growth simulation. Figure S3 shows the  
 1002 resulting number of cells at the last time point of a cycle over multiple growth-dilution cycles

1003 for the genotypes in @Figure S2. We can see that the adaptive lineages (blue curves) increase  
 1004 in abundance, while detrimental lineages (red curves) decrease.

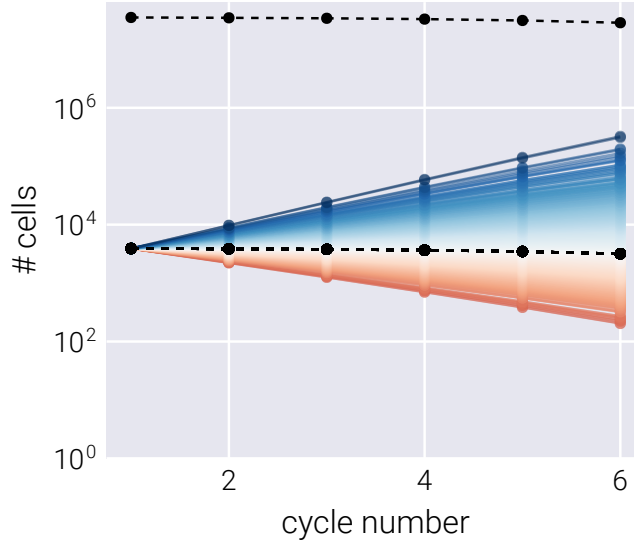


**Figure S3. Growth-dilution cycles for logistic growth simulation.** Each point represents the final number of cells after a growth cycle for each lineage. Colors are the same as in Figure S2.

1005 In Section , we derive the functional form to infer the relative fitness of each lineage as

$$\frac{1}{\tau} \ln \frac{f_{t+1}^{(b)}}{f_t^{(b)}} = (s^{(b)} - \bar{s}_t). \quad (\text{S107})$$

1006 Figure S4 shows the corresponding log frequency ratio curves for the logistic growth simulation.  
 1007 The displacement of these curves with respect to the neutral lineages determines the ground  
 1008 truth relative fitness value for these simulations.

1009 To simulate the experimental noise, we add two types of noise:

- 1010 1. Poisson noise between dilutions. For this, we take the final point of the logistic growth
- 1011 simulation and sample a random Poisson number based on this last point to set the
- 1012 initial condition for the next cycle.
- 1013 2. Gaussian noise when performing the measurements. When translating the underlying
- 1014 population composition to the number of reads, we can add a custom amount of
- 1015 Gaussian noise.

1016 Figure S5 shows the frequency trajectories (left panels) and log frequency ratios (right panels)  
 1017 for a noiseless simulation (upper panels) and a simulation with added noise (lower panels).  
 1018 The noiseless simulation is used to determine the relative fitness for each of the lineages,  
 1019 which serves as the ground truth to be compared with the resulting inference.

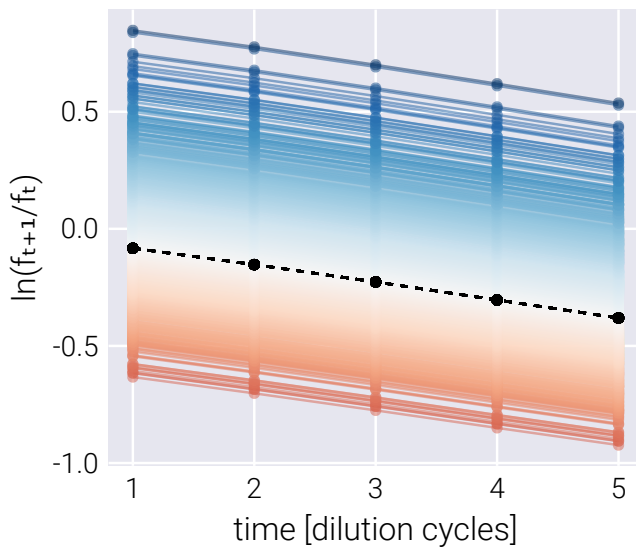


**Figure S4. Log frequency ratio for logistic growth simulations.** The relative distance of the color curves from the black dashed line determines the relative fitness of each lineage.

## 1020      Supplemental References

1021   <sup>25</sup>A. Gelman, D. Simpson, and M. Betancourt, “The Prior Can Often Only Be Understood in  
 1022   the Context of the Likelihood”, [Entropy 19, 555 \(2017\)](#).

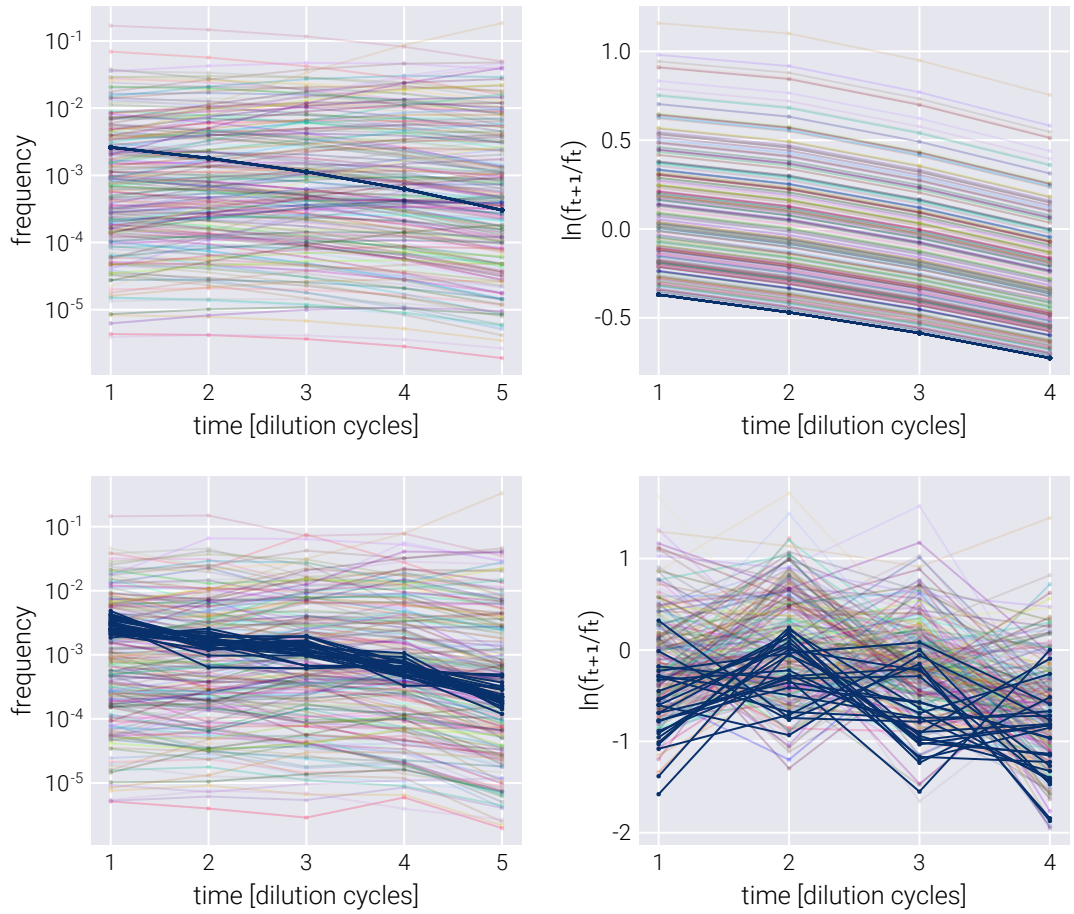


**Figure S5. Logistic growth-dilution simulations with and without noise**